Analysis of Dynamic Response of a Restraining System for a Powerless Advancing Ship Based on the Kane Method

Junyi Liu

College of Field Engineering, PLA University of Science and Technology, Nanjing 210007, PR China & Fluid Structure Interactions Research Group, University of Southampton, Southampton SO16 7QF, United Kingdom
E-mail: liujunyi_1988@outlook.com

Grant E Hearn

Fluid Structure Interactions Research Group, University of Southampton, Southampton SO16 7QF, United Kingdom
E-mail: g.e.hearn@soton.ac.uk

Xujun Chen *

College of Field Engineering, PLA University of Science and Technology, Nanjing 210007, PR China & China Ship Scientific Research Centre, Wuxi 214082, PR China
E-mail: chenxujun213@sina.com

Zhaobing Jiang

College of Field Engineering, PLA University of Science and Technology, Nanjing 210007, PR China
E-mail: owen9020@126.com

Guanghuai Wu

Nanjing Guangbo Engineering Technology co. LTD, Nanjing 210007, PR China
E-mail: wuguanghuai@sina.com

* Corresponding author.
E-mail addresses: chenxujun213@sina.com (X. Chen).

Analysis of Dynamic Response of a Restraining System for a Powerless Advancing Ship Based on the Kane Method

Abstract:

Following general explanations of the working principles of different existing retardation systems to restrain an advancing powerless ship the principles of a new overhead retardation system are presented. A two dimensional simplified model of the activated overhead system is formulated based on Huston's interpretation of the Kane methodology. Reduced Kane equations are used in the actual simulation, once initial conditions and mechanical analysis of constituent elements have been formulated. Having presented the computational process the various velocity, motion and joint constraint force characteristics of the anchor, the ship and the other elements are monitored in the time domain for the duration of the retardation process. Validation of the Kane based method is established utilising the conservation law and the Lagrangian based formulation of the retardation system within the ADAMS software. The results indicate that a peak value of constraint will occur because of the sudden movement of anchor and this peak is affected significantly by initial ship speed. Variation in anchor chain, overall cable length and its horizontal projected length has little influence upon retardation system performance, whilst the changes of sea bed friction, anchor mass, water depth, initial ship velocity and ship mass will make retardation behaviour different.

Keywords: Flexible ship restraining system; Ship transportation-bridge collision avoidance; Energy dissipated by ship-independent anchor; Kane method; Multibody Dynamics; Offshore Engineering

1. Introduction

As a consequence of increased cargo transportation with larger ships travelling at greater speeds collision risks have been raised between ships and above waterway transportation bridges. This has also led to more fatal collisions between ships and bridges (Mou et al. 2010; Yan and Dai 2011), which not only adversely affect traffic safety but also cause considerable losses. Therefore, research on ship collision with bridges has become an important international topic. The flexible collision-prevention devices have been focused on by an increasing number of researchers (Fan and Yuan 2014; Qiu et al. 2015) as rigid anti-collision devices can damage both the prevention devices and the colliding ship.

Wang et al. (2008) developed a flexible, energy-dissipating ship retardation device consisting of hundreds of steel-wire-rope coil (SWRC) connected in parallel and series. Zhou et al. (2012) analyzed the elastic behaviour of the retardation device by treating it as a circular elastic ring attached to a pile through elastic foundations. A non-dimensional parameter, corresponding to the ratio of the elastic foundation stiffness to the bending stiffness of the circular ring, was identified as important and a ratio was found to optimize the crashworthiness of the retreating structure. Wang et al. (2012) applied impact dynamics theory to illustrate how wave propagation and the dynamic behaviour of materials influence the impact force and energy transformation. The results generated illustrated that it was the material-dependent wave impedance that played a dominant role, rather than ship total mass and rigidity in determining the resulting impact force of ship and bridge.

Zhu et al. (2012) made several large-scale impact tests involving flexible pile-supported protective structures that absorbed impact energy through large deflections and yielding. The complexity of a three-dimensional analysis necessitated a simplified energy-based analysis method to estimate the lateral deflections. Comparison between

calculations and test measurements demonstrated that the simplified analysis method gave conservative results concerning the energy-absorbing capability.

A floating fender system can automatically adjust its elevation with the changes in water level.

Jiang and Chorzepa (2015) used an explicit nonlinear dynamic finite-element analysis program to evaluate the performance of a new floating fender system composed of fiber-reinforced plastic (FRP) box modules filled with rows of FRP tubes. The analysis indicated that the new fender system had excellent energy-absorbing capabilities, facilitated significantly smaller collision forces and increased collision duration imposed on the bridge pier and colliding ship. Jiang and Chorzepa (2016) applied the same analysis method to a floating fender based on different materials. In this case the floating steel fender system was primarily composed of readily available steel plate structures and rubber components. Because the proposed fender system extended the impact duration, the peak impact force between the bridge pier and the colliding vessel was notably reduced.

Wu et al. (2009) and Chen et al. (2009) researched a flexible floating collision-prevention system consisting of a string of surface buoys connected by cables. Each buoy is connected with a bottom slidable anchor. When the buoy arrangement is struck by a disabled ship, its kinetic energy is dissipated through the movement of the anchors. Chen et al. (2013) proposed the small balance method to determine the buoy position, anchor movement and the history of anchor chain forces due to ship collision with the flexible floating buoy blocking system. The predictions showed good agreements with model test measurements.

An overhead retardation system, mainly made up of gravity anchors and associated anchor chains connected at one end to a restraining net with supporting frames represents a new type of flexible ship collision prevention device. Its working principle is similar to an earlier floating buoy system investigated by Wu et al. (2009); Chen et al. (2009) and Chen et al. (2013). Such systems require precise determination of the dynamic characteristic of the anchor chains and restraining cables. This means that it is necessary to apply a multibody dynamic method to address such systems.

Recently Ku and Ha (2014), Xu et al. (2015), Tran and Kim (2015) and McNatt et al. (2015) have carried out multibody dynamic analysis within the context of offshore engineering applications. Similarly Chang et al. (2012) applied the multi-body dynamics approach to a single-point mooring buoy system consisting of a surface buoy, cable segments modelled as individual components and an anchor. Jiang et al. (2015) employed the homogeneous matrix method to model and simulate a four-body system with a floating base. The motions were analysed subject to wave and wind loads when the upper parts were spread sequentially or synchronously.

Based on the Kane method Shen et al. (2003) studied the rolling response of the ship in waves and the motion of a heavy load “synchro-slipping”. This approach was also adopted by Yang et al. (2014) to analyze the dynamic response of an underwater snake-like robot.

He et al. (2014) undertook the dynamic analysis of an offshore crane based on rigid-flexible coupling and the application of virtual prototyping-based multibody dynamics. After combining the computer software suites of ADAMS and ANSYS numerical calculations were carried out and model validity verified through comparison with experimental measurements.

However, the investigation of the dynamic response of anchor chain and restraining cable using multibody dynamic methods are rather scarce. This is particularly the case when addressing the condition of gravity anchor movements. Since the Kane method has the advantages of both vector and scalar based mechanics, it is applied in this paper to provide a preliminary analysis of the influence factors and system parameters on the responses of a powerless ship

restraining system.

Section 2 presents the working principle of a proposed ship restraining system together with its mathematical model. Then, mechanical analysis of the system and related solution methods are formulated in Section 3. Comparative studies of theoretical predictions and simulations are given in Section 4. Section 5 provides conclusions and paper closure.

2. Working principle of retardation system and its mathematical model

The proposed retardation system is concerned with stopping a powerless ship advancing into restricted water beyond a generally non-navigational bridge. The retardation system needs to be located upstream of the bridge at a distance commensurate with maximum stopping distance of ships using the waterway under consideration. The proposed overhead retardation system is introduced in Sub-section 2.1 together with an explanation of the underlying principles necessary to formulate the mathematical model addressed in other sub-sections.

2.1 Working principle of the overhead retardation system

The proposed retardation system is composed of an upper, middle and bottom restraining cable strung between two support frames and linked by vertical connection cables as illustrated in Figure 1. Depending upon the particular waterway to be investigated the total span of the bridge to be protected by the retardation system may need one or more of the described units.

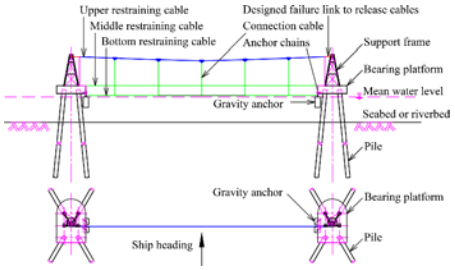

Figure 1. Front elevation and plan of a single unit of overhead retardation system

The middle and bottom cables exist so that smaller ships can trigger the retardation system. The arrangement of horizontal and vertical cables are collectively referred to as the “retardation net”. The upper restraining cable is kept in place by a secondary weak link connection at the top of each support frame. The continuation of the upper retraining cable beyond the weak link is connected to the end of the anchor chain. The chain is ultimately connected to the anchor. The middle and bottom cables have a weak link to the anchor chains. These links cannot sustain the anchor chain tension once the anchor has been released from the bearing platform. Therefore, if the ship makes contact with the middle or bottom cable, the weak connections with the anchor chains will fail. Hence the upper cable will be pulled downwards and break its associated weak links. Ship contact with the upper restraining cable also leads to the failure of the identified weak links. Hence the overhead net falling on to the deck of the ship is triggered by a ship making contact with upper, middle or bottom restraining cables. This paper does not address safety issues related to this reaction or subsequent operation of the retardation system.

A releasable concrete anchor and the associated studless anchor chain are stored on a ‘bearing’ platform identified in Figure 1. The support frame is fixed to the sea-bed or riveted by penetrating piles through the seabed. The restraining cable will begin to pull at the anchor chain once the ship has advanced sufficiently to allow the metal pin supporting the anchor to be dislodged from the bearing platform. The anchor will drop to the seabed or

riverbed.

When the restraining cables and anchor chains have become taught anchor dragging will commence and start to reduce the speed of advance of the ship. Ultimately the ship will be stopped as a consequence of the influence of the drag forces induced by the friction between the anchors and the seabed or the riverbed. The presence of any currents flowing against the ship will help to halt ship advance. Currents flowing in the same direction as the advancing ship could prevent the ship being stopped if the total drag forces are less than the current forces. Anchor sizing, in terms of weight and contact area with the seabed, needs to be selected to avoid the latter scenario described. This part of the design process is not detailed here, as it is a function of seabed characteristics and known local water flow rates.

To apply the Kane multibody dynamic analysis procedure the proposed retardation system will be simplified to permit a two dimensional (2D) rather than a 3D investigation.

2.2 Related assumptions for modelling

In order to demonstrate the Huston interpretation (Huston 1990) of the multibody analysis of Kane (Kane 1985), only the upper restraining cable of the net is considered, hence the retardation system is simplified to a 2D model with the net replaced with an auxiliary rod and a restraining cable connected to a length of anchor chain that is attached to a bottom mounted anchor, as illustrated in Figure 2. The anchor geometry is cuboid and the associated chain is treated as a sequence of homogenous elements with one chain link per element, whereas the single restraining cable is divided into three parts of differing lengths. Each cable portion is divided into homogeneous elements within each of the differing length. The seabed is treated as an elastic foundation beam model. The actual ship geometry is ignored and the ship is treated as a rigid box of dimensions consistent with actual ship length, beam and depth.

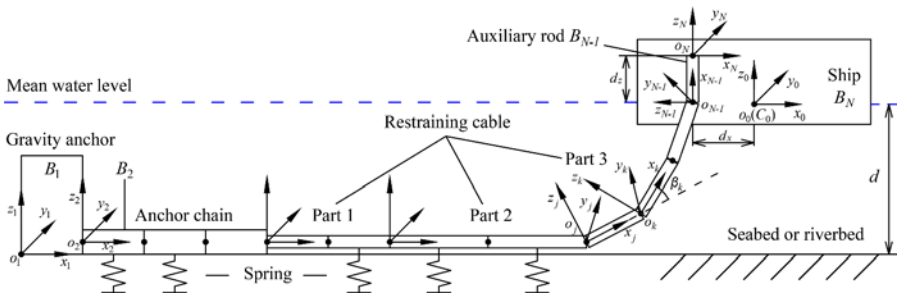

Figure 2. Two dimensional simplified physical model of retardation system

Application of this model requires additional assumptions to undertake the related calculations, namely:

(1) The period from ship impact with the retardation system to the release of the anchor from the bearing platform and the anchor falling to the seabed is not addressed within the calculation.

(2) Initially at time $t = 0$, the ship has an advancing velocity and the auxiliary rod rotates with it, whilst the connected cable and anchor chain are considered static. Hence the shape of the restraining cable is governed by the catenary equation. The cable has a uniform mass per unit length.

(3) Neighbouring elements of the chain and of the cable are free to move relative to one another without inducing any frictional effects.

(4) Links in the chain and the restraining cable are assumed to move devoid of friction along the seabed.

(5) The gravity anchor can only translate along the seabed; it has no other degrees of freedom.

(6) The sliding friction coefficient of anchor and seabed is assumed constant.

(7) Wind & wave influences are not addressed.

(8) Ship centroid is assumed to be located at the centre of the ship water plane.

2.3 Simplified mathematical model based on the Kane method

This section introduces the concepts necessary to implement the Huston interpretation of the Kane multibody analysis. In particular, the Huston (1990) suggested numbering of each object (body) within his branch method is adopted.

2.3.1 Two dimensional simplified physical model of retardation system

Within the two dimensional retardation system the gravity anchor is designated B_1 to indicate it is body number 1. Thereafter neighbouring bodies B_i are numbered consecutively with the last link (auxiliary rod) to the ship treated as object B_{N-1}. This link is initially considered to be fixed to the ship vertically, that is, perpendicular to the undisturbed free surface. The ship is thus referred to as body B_N. Each body 1 to N has its own local Cartesian reference system as indicated in Figure 2. Each element centroid is located at its geometric centre except for the ship which has its centre in the ship water plane as indicated in assumption (8).

The global inertial right-handed Cartesian coordinate system has origin o_0 located at the centre of the ship water plane. The positive x_0-axis points in the direction of ship advance and the positive z_0-axis points vertically upwards, as defined in Figure 2. The origin o_1 of the B_1 body-fixed coordinate system is located at the intersection of the vertical longitudinal plane of symmetry of the gravity anchor, the vertical aft face of the anchor and the flat horizontal seabed. The direction of the positive x_1-axis is forward along the anchor length, while the vertical z_1-axis is positive upwards.

The body-fixed coordinates of the homogeneous rods (representing the rigid links of the anchor chain, the rigid elements of the restraining cable and the auxiliary rod) are located at the hinge joints which connect neighbouring bodies. The x_k-axis is along the element and the orthogonal z_k-axis is upward and perpendicular to x_k. The ship is treated as an advancing cuboid whose body-fixed coordinate origin is the hinge joint linking the ship to the auxiliary rod. Initially the local coordinates of the ship are parallel to the inertial reference frame.

2.3.2 Transformation matrix and its derivative

The key point of applying the Kane method is to facilitate the study of the dynamic responses of a powerless ship and a proposed ship restraining system as a multibody situation. This necessitates establishing and solving the Kane equations for each body. Using the Kane terminology this means addressing the partial angular velocity, the partial velocity and the generalised speed of each constituent body. All of these quantities are closely related through the transformation matrices relating the body local coordinates to the inertial coordinate and their derivatives. Hence, the procedure for the specific calculation of the coordinate transformation matrices needs to be established first.

From the anchor of the restraining system to the ship each distinct body is treated as rigid. The k^{th} rigid body B_k

has its own set of Cardan angles $(\alpha_k,\ \beta_k,\ \gamma_k)$ between the rigid body B_k and its inner (adjacent) connecting rigid body B_j $(: j = k-1)$ to describe the position of rigid body B_k.

For a two-dimensional model of the retardation system angles α_k and γ_k are identically zero on each body. β_k is the angle subtended between the x_j-axis and x_k-axis and is thus the angle through which the rigid body B_k must be rotated to the orientation of B_j. This rotation is around the y_j-axis located at the lower end of the inner (adjacent) connecting body as illustrated in Figure 2. The sign of β_k is decided in accordance with the right-hand grip rule, that is positive or negative for clockwise and anticlockwise rotations respectively. The transformation matrix from B_k to B_j therefore has the simple form:

$$\boldsymbol{S}^{(jk)} = \begin{bmatrix} \cos\beta_k & 0 & \sin\beta_k \\ 0 & 1 & 0 \\ -\sin\beta_k & 0 & \cos\beta_k \end{bmatrix}. \tag{1}$$

Defining $\boldsymbol{n}_j$ and $\boldsymbol{n}_k$ as the unit vectors associated with the coordinate axes of the j^{th} and k^{th} bodies, it follows that $\boldsymbol{n}_j$ and $\boldsymbol{n}_k$ are square matrices of order 3 with each row defining the unit vector of each coordinate axis in turn. $\boldsymbol{n}_j$ and $\boldsymbol{n}_k$ are related through the defined rotation β_k and satisfy $\boldsymbol{n}_j = \boldsymbol{S}^{(jk)}\boldsymbol{n}_k$. Furthermore, $\boldsymbol{n}_{0m} : m = 1,2,3$ defines the unit vectors associated with each axis of the inertial reference system. When transforming time derivatives of angular velocity Huston (1990) has noted that the associated general transformations for general angles $(\alpha_k,\ \beta_k,\ \gamma_k)$ can become singular. This difficulty can be overcome through introduction of the Euler parameters. The Euler parameters for our 2D-formulation can be simplified as follows:

$$\varepsilon_{k1} = \varepsilon_{k3} = 0,\ \ \varepsilon_{k2} = \pm\sin(\beta_k/2) \text{ and } \varepsilon_{k4} = \cos(\beta_k/2). \tag{2}$$

Hence application of cosine and sine double angle relationships means the transformation matrix $\boldsymbol{S}^{(jk)}$ assumes the alternative form:

$$\boldsymbol{S}^{(jk)} = \begin{bmatrix} 2\varepsilon_{k4}^2 - 1 & 0 & 2\varepsilon_{k2}\varepsilon_{k4} \\ 0 & 1 & 0 \\ -2\varepsilon_{k2}\varepsilon_{k4} & 0 & 2\varepsilon_{k4}^2 - 1 \end{bmatrix}. \tag{3}$$

The transformation matrix $\boldsymbol{S}^{(0k)}$ from rigid body B_k to the inertial coordinate system can be obtained through repeated application of the pertinent transformation matrices over the sequential path linking B_k to the inertial coordinate system. That is:

$$\boldsymbol{S}^{(0k)} = \prod_{w=0}^{k-1} \boldsymbol{S}^{(wv)} \ : v = w + 1. \tag{4}$$

The Cardan angles between the rigid body B_k and the inertial coordinate are given by:

$$\beta_{0k} = \arcsin S_{13}^{(0k)}. \tag{5}$$

Here the subscript 13 indicates the appropriate matrix element.

At the initial time $t = 0$ the angles associated with the chain related bodies are zero and the angles between contiguous members of the restraining cable are determined through application of the appropriate catenary equations. Hence the transformation matrix $\boldsymbol{S}^{(jk)}$ from B_k to B_j for each pair of indices (j, k) can be calculated by applying Equation (3) with the definitions of the Euler parameters provided by Equation (2). Thereafter $\boldsymbol{S}^{(0k)}$ is determined by applying Equation (4). Equation (5) can be used to determine the rotation of the bodies in the system

and hence the current profile of the constituent bodies.

In subsequent numerical calculations new values of the Euler parameters will be required to generate an updated value of $\boldsymbol{S}^{(0k)}$. To achieve this task, generalised speeds & generalised coordinates are to be introduced in Section 2.3.3 together with updates of partial angular velocity & partial velocity components as addressed in Section 2.3.4. Thereafter, new Euler parameter values are derived through solution of the first order differential equations formulated in Section 2.3.5.

These differential equations require derivatives of the transformation matrices. It can be shown (following some mathematical dexterity) that the element 'in' of $\dot{\boldsymbol{S}}^{(0k)}$ satisfies:

$$\dot{S}_{in}^{(0k)} = -e_{irm}\omega_m^{(0k)}S_{rn}^{(0k)} \quad : i,r,m,n = 1,2,3. \tag{6}$$

Here, r & m are repeated indices; $\omega_m^{(0k)}$ are the components of the absolute angular velocity $\boldsymbol{\omega}^{(0k)}$ of rigid body B_k with respect to the inertial reference frame. e_{irm} are the permutation coefficients defined by:

$$e_{irm} = (i-r)(r-m)(m-i)/2 \quad : i,r,m = 1,2,3. \tag{7}$$

There are only 6 non-zero values of e_{irm} corresponding to the conditions $i \neq r, r \neq m$ & $m \neq i$.

2.3.3 Generalised speeds and generalised coordinates

The number of the degrees of freedom (DOF) within the system determines the number of governing equations. As the restraining system consists of N rigid bodies, it has at most 3N translational degrees of freedom and 3N rotational degrees of freedom. In the Huston implementation of the Kane formulation the generalised speeds $\dot{x}_l$ are defined in terms of the angular velocity components ω_{ki} between B_k and its inner connecting body or the relative velocity components $\dot{s}_{ki}$ of adjacent rigid bodies, that is:

$$\dot{x}_l = \begin{cases} \omega_{ki} & l = 3(k-1)+i \\ \dot{s}_{ki} & l = 3(N+k-1)+i \end{cases} : k = 1,2,\dots,N \;\&\; i = 1,2,3. \tag{8}$$

With respect to the restraining system the fact that rotation can only take place about the local y-axes and only the anchor can translate means that the non-zero generalised speeds are ω_{k2} and $\dot{s}_{11}$.

The generalised speeds $\dot{x}_l$ correspond to the derivatives of relative movements between the rigid bodies. It would therefore be reasonable to take the relative translations as the generalised coordinates to describe the position of each of the rigid bodies. However, there are no generalised coordinates whose derivatives readily equate to the components of relative angular velocity. Therefore the generalised speeds must be expressed in terms of the derivatives of other available coordinates. Euler parameters introduced earlier in Equation (2) as generalised coordinates fulfil the required role.

2.3.4 Partial angular velocity component and partial velocity component

The angular velocity and velocity of any member body can be determined from a linear combination of generalised speeds (Huston 1990).

The angular velocity $\boldsymbol{\omega}^{(0k)}$ is written as:

$$\boldsymbol{\omega}^{(0k)} = \omega_{klm}\dot{x}_l\boldsymbol{n}_{0m} \quad : k = 1,2,\dots,N; \;\; l = 1,2,\dots,6N \;\&\; m = 1,2,3. \tag{9}$$

Here, l is a repeated index; $\boldsymbol{n}_{0m}$ are mutually perpendicular inertial reference frame fixed unit vectors and the partial angular velocity components ω_{klm} satisfy:

$$\omega_{klm} = \begin{Bmatrix} \delta_{ml} & : l = 1,2,3 \\ 0 & : l = 4,5,\dots 6N \end{Bmatrix} k = 1$$
$$\begin{Bmatrix} \omega_{jlm} & : l = 1,2,\dots 3(k-1) \\ S_{mp}^{(0j)} & : l = 3k-2,3k-1,3k;\ p = l-(3k-3) \\ 0 & : l = 3k+1,3k+2,\dots 6N \end{Bmatrix} k = 2,3,\dots,N\ \&\ j = k-1 \quad . \tag{10}$$

Here, δ_{ml} is the Kronecker delta function with its usual definition of:

$$\delta_{ml} = \begin{cases} 1 & : m = l \\ 0 & : m \neq l \end{cases} : m,l = 1,2,3. \tag{11}$$

The time derivatives of ω_{klm}, obtained by differentiating Equation (10), clearly satisfy:

$$\dot{\omega}_{klm} = \begin{Bmatrix} 0 & : l = 1,2,3,\dots,6N;\ \ k = 1 \\ \dot{\omega}_{jlm} & : l = 1,2,\dots 3(k-1) \\ \dot{S}_{mp}^{(0j)} & : l = 3k-2,3k-1,3k;\ p = l-(3k-3) \\ 0 & : l = 3k+1,3k+2,\dots 6N \end{Bmatrix} k = 2,3,\dots,N\ \&\ j = k-1. \tag{12}$$

The determination of the corresponding expression for the partial velocity components requires appreciation of variables defined in Figure 3. In particular Q_k is a fixed point in B_j corresponding to the joint between body B_k and its inner connecting body B_j.

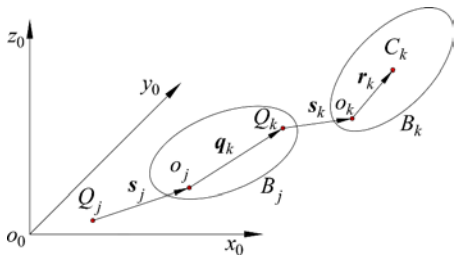

Figure 3. Objects in the path and relevant vectors

The position vector of Q_k is $\boldsymbol{q}_k$ in the B_j body-fixed local coordinate system with origin o_j ($j = k-1$). Its coordinates are denoted by $q_{kn} : n = 1,2,3$. The vector $\boldsymbol{s}_k$ with components s_{kn} in the B_j body-fixed reference system describes the relative translation of B_k relative to B_j. $\boldsymbol{s}_k$ is only pertinent when Q_k and o_k are capable of moving relative to one another. For neighbouring bodies modelling a continuum of an inelastic material these points are coincident. The position vector of the centroid C_k of B_k relative to the origin o_k is $\boldsymbol{r}_k$ and its coordinates are denoted by $r_{kn} : n = 1,2,3$.

Assuming that $\boldsymbol{p}_k$ is the vector position of C_k relative to the fixed inertial reference system with origin o_0 then application of relevant transformations means that:

$$\boldsymbol{p}_k = \boldsymbol{r}_k + \sum_{w=0}^{k-1}[\boldsymbol{q}_v + \boldsymbol{s}_v] \equiv \left[S_{mn}^{(0k)} r_{kn} + \sum_{w=0}^{k-1} S_{mn}^{(0w)}(q_{vn} + s_{vn})\right]\boldsymbol{n}_{0m} : m,n = 1,2,3\ \&\ v = w+1. \tag{13}$$

Defining $\boldsymbol{v}^{(0k)} = \dot{\boldsymbol{p}}_k = \mathrm{d}\boldsymbol{p}_k/\mathrm{d}t$, it can be established (Huston 1990) that:

$$\boldsymbol{v}^{(0k)} = v_{klm}\dot{x}_l \boldsymbol{n}_{0m} : k = 1,2,\dots,N;\ l = 1,2,\dots,6N\ \&\ m = 1,2,3 \tag{14}$$

and v_{klm} is defined in accordance with:

$$v_{klm} = \begin{cases} \sum_{w=0}^{k-1} \left[e_{irm} \omega_{wli} S_{rn}^{(0w)} (q_{vn} + s_{vn}) \right] + e_{irm} \omega_{kli} S_{rn}^{(0k)} r_{kn} & : v = w+1 \;\&\; k = 1,2,\dots,N \\ 0 & : l = 3k+1, 3k+2, \dots, 3N \;\&\; k = 1,2,\dots,N \\ \omega_{k(l-3N)m} & : l = 3N+1, 3N+2, \dots, 6N \;\&\; k = 1,2,\dots,N \end{cases}. \quad (15)$$

The time derivatives of the partial velocity components provided in Equation (15) are:

$$\dot{v}_{klm} = \begin{cases} \sum_{w=0}^{k-1} \left[e_{irm} \dot{\omega}_{wli} S_{rn}^{(0w)} (q_{vn} + s_{vn}) + e_{irm} \omega_{wli} \dot{S}_{rn}^{(0w)} (q_{vn} + s_{vn}) + e_{irm} \omega_{wli} S_{rn}^{(0w)} \dot{s}_{vn} \right] \\ \quad + e_{irm} (\dot{\omega}_{kli} S_{rn}^{(0k)} r_{kn} + \omega_{kli} \dot{S}_{rn}^{(0k)} r_{kn}) & : v = w+1;\; l = 1,2,\dots,3k \;\&\; k = 1,2,\dots,N \\ 0 & : l = 3k+1, 3k+2, \dots, 3N \;\&\; k = 1,2,\dots,N \\ \dot{\omega}_{k(l-3N)m} & : l = 3N+1, 3N+2, \dots, 6N \;\&\; k = 1,2,\dots,N \end{cases}. \quad (16)$$

For the two dimensional restraining system model, all the values of s_{vn} & $\dot{s}_{vn}$ are zero except for s_{11} & $\dot{s}_{11}$ related to anchor translation and associated anchor velocity.

2.3.5 Reduced Kane's equation

The formulation details of the previous section provide the means to determine centroid velocity together with the angular velocity of B_k through the partial velocity components, partial angular velocity components and generalised speeds. Their derivatives are expressed next as:

$$\dot{\boldsymbol{v}}^{(0k)} \equiv \boldsymbol{a}_k = (v_{klm}\ddot{x}_l + \dot{v}_{klm}\dot{x}_l)\boldsymbol{n}_{0m} \;\&\; \dot{\boldsymbol{\omega}}^{(0k)} \equiv \boldsymbol{\alpha}_k = (\omega_{klm}\ddot{x}_l + \dot{\omega}_{klm}\dot{x}_l)\boldsymbol{n}_{0m}. \quad (17)$$

In our two-dimensional model of the restraining system the anchor ($k = 1$) and ship ($k = N$) are perceived as cuboid in shape and to be of length, width & height designated L_k, w_k, h_k whereas the discrete bodies representing a mooring chain link or an element of the restraining cable are treated as rods of length L_k and radius R_k. d_S is the vertical distance from the ship geometrical centre to the water plane. Throughout the associated mass of the k^{th} body is m_k. Hence the inertia dyadic matrix associated with the centroid of the body B_k can be written as:

$$\boldsymbol{I}_k^C = \begin{cases} \frac{m_k}{12} \begin{bmatrix} w_k^2 + h_k^2 & 0 & 0 \\ 0 & L_k^2 + h_k^2 & 0 \\ 0 & 0 & L_k^2 + w_k^2 \end{bmatrix} & : k = 1 \\ m_k \begin{bmatrix} R_k^2/2 & 0 & 0 \\ 0 & L_k^2/12 & 0 \\ 0 & 0 & L_k^2/12 \end{bmatrix} & : k = 2,3,\dots,N-1. \\ \frac{m_k}{12} \begin{bmatrix} w_k^2 + h_k^2 + 12d_S^2 & 0 & 0 \\ 0 & L_k^2 + h_k^2 + 12d_S^2 & 0 \\ 0 & 0 & L_k^2 + w_k^2 \end{bmatrix} & : k = N \end{cases} \quad (18)$$

Hence the inertia matrix of B_k in the inertia reference frame is:

$$\boldsymbol{I}_k = \left(\boldsymbol{S}^{(0k)}\right)^{\mathrm{T}} \boldsymbol{I}_k^C \boldsymbol{S}^{(0k)}. \quad (19)$$

Next denoting by $I_{kmn} : k = 1,2,\dots,N$ the mn^{th} element of $\boldsymbol{I}_k$ for body B_k in the inertia reference frame, then the expansion of the inertia force $\boldsymbol{F}_k^*$ and the inertial moment $\boldsymbol{T}_k^*$, according to Section 7.5 of Huston (1990), satisfy:

$$\boldsymbol{F}_k^* = -m_k\boldsymbol{a}_k = -m_k(v_{klm}\ddot{x}_l + \dot{v}_{klm}\dot{x}_l)\boldsymbol{n}_{0m}$$
and
$$\boldsymbol{T}_k^* = -\boldsymbol{I}_k\cdot\boldsymbol{\alpha}_k - \boldsymbol{\omega}_k\times(\boldsymbol{I}_k\cdot\boldsymbol{\omega}_k) = -[I_{kmn}(\omega_{klm}\ddot{x}_l + \dot{\omega}_{klm}\dot{x}_l) + e_{rsm}\omega_{klr}\omega_{kpn}I_{ksn}\dot{x}_l\dot{x}_p]\boldsymbol{n}_{0m}. \quad (20)$$

Defining F_{km}^* and T_{km}^* as the resolved components of $\boldsymbol{F}_k^*$ and $\boldsymbol{T}_k^*$ with respect to the inertial reference system $\boldsymbol{n}_0$ the generalised inertia force on body B_k is:

$$F_l^* = v_{klm}F_{km}^* + \omega_{klm}T_{km}^*. \quad (21)$$

Hence the total generalised inertia force acting on the whole restraining system (including anchor & ship) is:

$$F_l^* = -m_k v_{klm}\left(v_{kpm}\ddot{x}_p + \dot{v}_{kpm}\dot{x}_p\right) - I_{kmn}\omega_{klm}\left(\omega_{kpm}\ddot{x}_p + \dot{\omega}_{kpm}\dot{x}_p\right) - I_{ksn}\omega_{klm}e_{rsm}\omega_{kpr}\omega_{kqn}\dot{x}_p\dot{x}_q \quad (22)$$
$$: m,n,r,s = 1,2,3;\ \ p,q,l = 1,2,\dots,6N\ \&\ k = 1,2,\dots,N.$$

The "active" forces experienced by B_k are due to the external forces and the reaction of the inner body and/or the outer body on B_k. Let F_{km} and T_{km} represent the components of active force $\boldsymbol{F}_k$ and active moment $\boldsymbol{T}_k$ with respect to inertial reference system $\boldsymbol{n}_0$. Then the generalised active forces are expressed as:

$$F_l = v_{klm}F_{km} + \omega_{klm}T_{km} \ : l = 1,2,\dots,6N;\ k = 1,2,\dots,N\ \&\ m = 1,2,3\,. \quad (23)$$

The assumptions and constraints introduced in Section 2.2 are consistent with the assumption that relative motions between elements of the multibody restraining system make no contribution to the generalised active forces.

Kane equations can be deduced from the virtual work principle and expressed as (Kane 1985):

$$F_l + F_l^* = 0. \quad (24)$$

Substitution of Equations (22) & (23) into Equation (24) and rearranging leads to:

$$a_{lp}\ddot{x}_p = F_l - \left(m_k v_{klm}\dot{v}_{kpm}\dot{x}_p + I_{kmn}\omega_{klm}\omega_{kpm}\dot{x}_p + I_{ksn}\omega_{klm}e_{rsm}\omega_{kpr}\omega_{kqn}\dot{x}_p\dot{x}_q\right) \equiv f_l \quad (25)$$
$$: m,n,r,s = 1,2,3;\ \ p,q,l = 1,2,\dots,6N;\ \ k = 1,2,\dots,N$$

with

$$a_{lp} = m_k v_{klm}v_{kpm} + I_{kmn}\omega_{klm}\omega_{kpm}. \quad (26)$$

Here, k is a repeated index. Equation (25) is suitable for the general open loop-tree system in which each body has six degrees of freedom. As the number of degrees of freedom lessens so the number of variables to be determined reduces correspondingly. For constant generalised speeds the derivatives $\partial\boldsymbol{\omega}_k/\partial\dot{x}_l$ and $\partial\boldsymbol{v}_k/\partial\dot{x}_l$ vanish. Thus calculation of a generalised force is only valid for undetermined generalised speeds.

For the two dimensional restraining system the derived Kane equations are readily simplified. The generalised speed of the anchor, $\dot{x}_{3N+1}$, is dependent upon the state of the anchor and the forces the anchor experiences. In particular, $\dot{x}_{3N+1}$ is zero if the anchor is stationary and the sum of the tension and the drag force experienced by the anchor is less than the frictional force between anchor and seabed. If the sum of the tension and the drag force exceeds the frictional force or the anchor velocity is non-zero, the degree of freedom corresponding to $\dot{x}_{3N+1}$ is considered to be released.

Each constituent body (other than the anchor) can only rotate around the y_0-axis, hence when the anchor remains in its initial seabed location or ceases to move, it follows that $\dot{x}_l \neq 0 : l = 5,8,11,\dots,3N-1$. Otherwise, it follows that $\dot{x}_l \neq 0 : l = 5,8,11,\dots,3N-1\ \&\ 3N+1$. Taking the latter condition, as an example, the reduced Kane equations to be solved are:

$$a_{lp}\ddot{x}_p = f_l \quad : l, p = 5, 8, 11, \dots, 3N-1 \;\&\; 3N+1. \tag{27}$$

Equation (27) is a nonlinear first-order ordinary differential equation group having *N* equations with respect to the generalised speeds $\dot{x}_l$.

Equation (27) implicitly contains other variables to be determined to facilitate determination of the generalised speeds $\dot{x}_l$. Assignment of elements of the partial velocity components v_{klm} and their derivatives $\dot{v}_{klm}$ are based on Equations (15) & (16), whereas the partial angular velocity components are provided through Equations (10) & (12). The elements of the inertial matrix $\boldsymbol{I_k}$ are generated using Equations (4), (18) & (19). The permutation coefficients e_{irm} are defined by Equation (7). The Euler parameters for our general 2D-formulation are provided by Equation (2). However, for the two dimensional restraining system since there are no rotations about the local x and z-axes it follows that:

$$\dot{\varepsilon}_{k1} = 0, \dot{\varepsilon}_{k2} = \varepsilon_{k4}\omega_{k2}/2, \dot{\varepsilon}_{k3} = 0 \text{ and } \dot{\varepsilon}_{k4} = -\varepsilon_{k2}\omega_{k2}/2 \quad : k = 1,2, \dots N. \tag{28}$$

Equation (28) provides $2N$ first-order differential equations with respect to the Euler parameters ε_{k2} & ε_{k4}. Appealing to Equation (8) and its associated comments, the relationship between the movement variables and the generalised speeds is:

$$\dot{s}_{11} = \dot{x}_{3N+1}. \tag{29}$$

Combining the Equations (27), (28) and (29) yields $(3N+1)$ closed first-order differential equations, in which the undetermined variables are $\dot{x}_l \;: l = 5, 8, 11, \dots, 3N-1 \;\&\; 3N+1$, ε_{k2} & $\varepsilon_{k4} \;: k = 1, 2, \dots, N$ and s_{11}.This list of generalised speeds do not involve $\dot{x}_{3N+1}$ & s_{11} at those time steps when the anchor remains in its initial seabed location or ceases to move. The equations can be solved through application of the Runge-Kutta procedure. The core task is computation of the transformation matrices and the four basic kinematic arrays associated with the partial angular velocity components, the partial velocity components and their respective derivatives at each time step.

3. Solution method

The forces and the moments exerted on the restraining system influence the behaviour of the system. Hence they must be determined at each instant in time as the solution of the Kane equations set out in Section 2 is advanced. Prior to seeking the time dependent solution the initial state of the restraining system is defined.

3.1 Initial configuration of system

The initial time of the simulation corresponds to the ship maintaining a steady course shortly after mechanical engine failure, which leads to anchor dropping with anchor chain and restraining cable payout taking place. The top side of the restraining cable is connected to a rod free to rotate in a vertical plane as indicated earlier in Figure 2. An approximate location of the cuboid anchor is assumed with the anchor chain maintaining contact with the flat horizontal seabed vertically below the path of ship passage, whereas the restraining cable is long enough to continue the straight line of the anchor chain links and so can be treated as a complete catenary of uniform mass per unit length, as sketched in Figure 4.

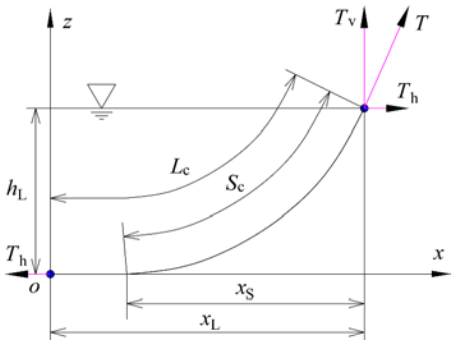

Figure 4. Complete catenary

The lower end point of the restraining cable is located at the point *o*. The upper tension imposed by the auxiliary element is T with horizontal and vertical resolved components T_h and T_v. The restraining cable is of overall length L_c and weight w_c per unit length in the sea. The length, vertical and horizontal projections of the non-horizontal portion of the cable are S_c, h_L and x_S respectively, whereas x_L is the horizontal projection of L_c on the seabed. Defining $a = T_h/w_c$ and $b = x_S/a$ the standard catenary equations lead to the relationships:

$$(\cosh(b) - 1)(L_c - x_L) = h_L(\sinh(b) - b), \quad (30)$$

$$T_h = w_c(L_c - x_L)/(\sinh(b) - b), \quad (31)$$

$$T_v = T_h \cdot \sinh(b), \quad (32)$$

$$h_L = a(\cosh(x_S/a) - 1) \text{ and} \quad (33)$$

$$S_c = a \cdot \sinh(b) = a \cdot \sinh(x_S/a). \quad (34)$$

Since the parameters w_c, L_c, x_L and h_L are known at the initial time, then b can be determined from Equation (30). Hence T_h & T_v are immediately determinable from Equations (31) & (32) respectively. Hence a is readily evaluated and h_L & S_c determined from Equations (33) & (34) in turn.

Next, the initial coordinates (X_k, Y_k, Z_k) of the restraining cable element B_k, corresponding to the origin of the element's local coordinate system, can be determined. Let L_L represent the length of some selected point on the restraining cable from the origin. If $L_L < x_L - x_S$ then the point is located on the portion of cable in contact with the seabed and therefore $X_k = L_L, Z_k = 0$ & $Y_k = 0$. Otherwise the selected point lies on the actual catenary and thus $L_L \geq x_L - x_S$ and assigning the left side of the Equation (34) to $S_{ck} = L_L - x_L + x_S$ will provide x_{Sk} and so the abscissa $X_k = x_L - x_S + x_{Sk}$, whereas substitution of x_{Sk} into Equation (33) determines Z_k. Throughout $Y_k = 0$. Let N_A represent the quantity of anchor chain elements, then the angle subtended between the k^{th} restraining cable element and the x_0-axis is:

$$\beta_{0k} = -\arctan\left(\frac{Z_{k+1} - Z_k}{X_{k+1} - X_k}\right) \; : k = N_A + 2, \ldots, N - 2. \quad (35)$$

3.2 Mechanical analysis of system

This section provides required details related to earlier identified 'active' forces.

3.2.1 Forces on gravity anchor

The forces acting on the gravity anchor are the weight G_1, the buoyancy F_1^B, the seabed reaction force F_1^S, the frictional force F_1^F, the fluid drag force F_1^D and the tension F_2^H exerted by the anchor chain as illustrated in Figure

5.

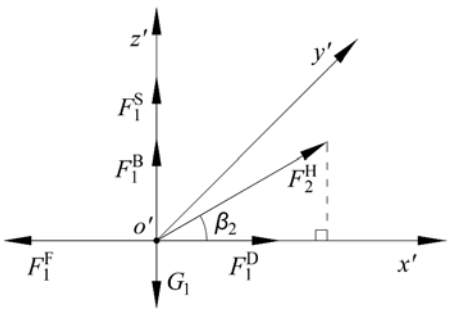

Figure 5. Forces on gravity anchor

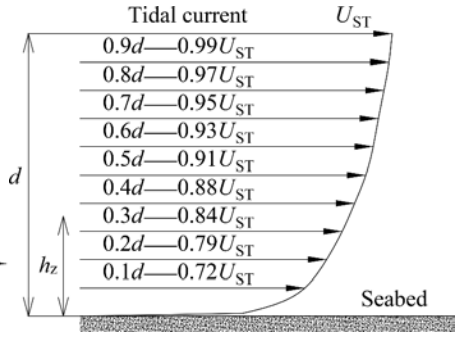

Figure 6. Tidal current velocity profile

The gravity anchor is assumed to move along the flat horizontal seabed, and its vertical movement is not considered. Define a_{1x} as the horizontal acceleration of the anchor along the *x*-direction, then equilibrium in the horizontal direction implies:

$$m_1 a_{1x} = F_2^H \cos\beta_2 - F_1^F + F_1^D. \tag{36}$$

If the friction coefficient between the seabed and the gravity anchor is μ; the density of the seawater is ρ; the displaced volume of the anchor is V_1; the gravitational acceleration is g, then the sliding friction can be expressed as:

$$F_1^F = \mu\left(m_1 g - \rho V_1 g - F_2^H \sin\beta_2\right). \tag{37}$$

If the anchor horizontal velocity $v_1^{(01)} = 0$ & $F_2^H \cos\beta_2 - F_1^F + F_1^D \le 0$, the anchor is assumed to be temperately fixed on the seabed; if not, the sliding force exists and the anchor is considered to have a degree of freedom along the x_0-axis. When the anchor moves, the sliding friction value is calculated based on the tension F_2^H obtained at the previous time step.

Generally, the sea current consists of the tidal current and the wind drift current. There are many degrees of randomness associated with the wind drift current, so only the tidal current is considered in this paper. A representative tidal current velocity profile (Wang 2004) is depicted in Figure 6. h_z is the distance of a current specification point from the seabed; U_{ST} is the flow velocity at the sea water free surface and d is the sea water depth. U_{hT} is the current velocity at h_z that is:

$$U_{hT} = U_{ST}\left(\frac{h_z}{d}\right)^{\frac{1}{7}}. \tag{38}$$

Let C_1^D represent the drag coefficient for the gravity anchor and U_1 denote the current velocity relative to the anchor centroid, then the anchor drag force is:

$$F_1^D = C_1^D \rho w_1 h_1 U_1 |U_1|/2. \tag{39}$$

According to Saleh (2002), $C_1^D = 1.05$ is a representative value of drag coefficient.

3.2.2 Forces on rod

The possible forces experienced by a chain or restraining cable element are shown in Figure 7. The actual forces

involved will depend on whether the element is in contact with or located above the seabed. Each element of anchor chain and restraining cable $B_k : k = 2,3,\dots,N-2$ is mainly affected by the element weight G_k, the reaction force F_k^{S} due to the seabed contact, the buoyancy F_k^{B}, the tangential drag force F_k^{V}, the added mass force F_k^{A} and the normal drag force F_k^{D}. The resultant forces F_k^{A} and F_k^{D} are determined by integrating their partial contributions F_k^{AE} & F_k^{DE} at different locations along the element. These variations of elemental inertial and drag forces lead to corresponding contributions of added mass torque T_k^{A} and drag torque T_k^{D}. The associated tensions at the lower and upper ends of the element are designated $-F_k^{\mathrm{H}}$ and F_{k+1}^{H} respectively as illustrated in Figure 7. The auxiliary rod is assumed to be above the free surface and thus the forces acting on it only include the weight G_{N-1} and the associated tensions at the lower and upper ends ($-F_{N-1}^{\mathrm{H}}$ & F_N^{H}). Let w_{d} represents the dry weight of unit length of each rod element, then the weight of B_k can be expressed as:

$$G_k = w_{\mathrm{d}} L_k : k = 2,3,\dots,N-1. \tag{40}$$

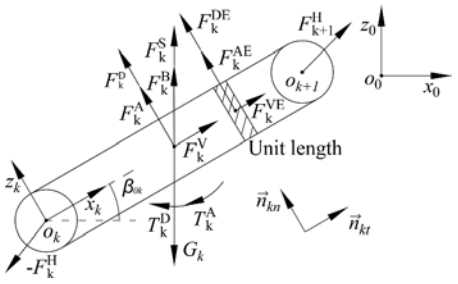

Figure 7. Forces on rod

It is possible that an anchor chain or restraining cable element can become partially embedded in the seabed. In this case let V_k^{S} denote the volume of the element embedded in the seabed and the normal counter-force coefficient of the foundation of seabed is designated as k_z. For a soft soil $k_z = 5 \times 10^6 \mathrm{N \cdot m^{-3}}$ (Ma et al. 2012) and hence the supporting force acting on B_k is:

$$F_k^{\mathrm{S}} = k_z V_k^{\mathrm{S}}. \tag{41}$$

The buoyancy expression is simply:

$$F_k^{\mathrm{B}} = \rho(V_k - V_k^{\mathrm{S}})g \ : k = 2,3,\dots,N-2. \tag{42}$$

The normal and tangential current velocities are v_{kn} and v_{kt} relative to selected point of the body B_k. $\dot{v}_{kn}$ is the partial time derivative of v_{kn} used as an estimator of the local acceleration. U_k is the normal water velocity relative to the centroid of body B_k, and $\dot{U}_k$ is its corresponding time derivative. The local velocities and accelerations are related to their corresponding inertial frame quantities via the following transformations:

$$[v_{kt}, 0, U_k]^{\mathrm{T}} = -\left[\boldsymbol{S}^{(0k)}\right]^{\mathrm{T}} \left[v_1^{(0k)} - U_{\mathrm{hT}}, 0, v_3^{(0k)}\right]^{\mathrm{T}}$$

and (43)

$$\left[\dot{v}_{kt}, 0, \dot{U}_k\right]^{\mathrm{T}} = -\left[\boldsymbol{S}^{(0k)}\right]^{\mathrm{T}} \left[\dot{v}_1^{(0k)}, 0, \dot{v}_3^{(0k)}\right]^{\mathrm{T}}.$$

The diameter of each element is $D_k = 2R_k$. Next let C_{M} denote the added mass coefficient, C_{D} the normal drag coefficient and C_{F} the tangential drag coefficient. The values of these coefficients in our model are: $C_{\mathrm{M}} = 1$,

$C_{\mathrm{D}} = 1.21$ and $C_{\mathrm{F}} = 0.062$ (Huston 1981). $\vec{n}_{kn}$ and $\vec{n}_{kt}$ are the normal and tangential unit vectors of current velocity indicated in Figure 7. Hence the partial elemental tangential drag force, the normal added mass force and the drag force per unit length are expressible as:

$$\begin{aligned} F_k^{\mathrm{VE}} &= \pi\rho D_k C_{\mathrm{F}} v_{kt}^2 \vec{n}_{kt}/2, \\ F_k^{\mathrm{AE}} &= \pi\rho D_k^2 C_{\mathrm{M}} |\dot{v}_{kn}| \vec{n}_{kn}/4 \text{ and} \\ F_k^{\mathrm{DE}} &= \rho D_k C_D v_{kn}^2 \vec{n}_{kn}/2. \end{aligned} \tag{44}$$

The resultant forces and torques acting on the centroid of body are determined by integration of the elemental forces along the length of the cable or chain element using Equation (44). That is, dropping each associated unit normal, since direction of action is readily appreciated, it may be shown that:

$$\begin{cases} F_k^{\mathrm{v}} = sign(v_{kt})\pi\rho D_k L_k C_{\mathrm{F}} v_{kt}^2/2 \\ T_k^{\mathrm{v}} = 0 \end{cases}, \tag{45}$$

$$\begin{cases} F_k^{\mathrm{A}} = \pi\rho D_k^2 C_{\mathrm{M}} \dot{U}_k L_k/4 \\ T_k^{\mathrm{A}} = -\pi\rho D_k^2 C_{\mathrm{M}} \dot{\omega}_2^{(0k)} L_k^3/48 \end{cases} \text{ and} \tag{46}$$

$$\begin{cases} F_k^{\mathrm{D}} = sign(U_k)\rho D_k C_{\mathrm{D}} [U_k^2 L_k + (\omega_2^{(0k)})^2 L_k^3/12]/2 \\ T_k^{\mathrm{D}} = -sign\left(\omega_2^{(0k)}\right)\rho D_k C_{\mathrm{D}} \left|U_k \omega_2^{(0k)}\right| L_k^3/12 \end{cases} : |U_k| \geq \left|\omega_2^{(0k)}\right| L_k/2$$

$$\begin{cases} F_k^{\mathrm{D}} = \rho D_k C_{\mathrm{D}} \left[\dfrac{U_k^3}{3\left|\omega_2^{(0k)}\right|} + \dfrac{U_k \left|\omega_2^{(0k)}\right| L_k^2}{4}\right] \\ T_k^{\mathrm{D}} = -sign\left(\omega_2^{(0k)}\right)\rho D_k C_{\mathrm{D}} \left[\dfrac{\left(\omega_2^{(0k)}\right)^2 L_k^4}{64} + \dfrac{U_k^2 L_k^2}{8} - \dfrac{U_k^4}{12\left(\omega_2^{(0k)}\right)^2}\right] \end{cases} : |U_k| < \left|\omega_2^{(0k)}\right| L_k/2 \tag{47}$$

The procedure for calculating the constraint forces at the hinge joints is based on Huston (1990) and is summarized next.

The first step is to determine the generalised constraint forces acting on the rigid body centroid assuming that the hinge joint constraints are temporarily removed. These generalised forces experienced by body B_k, under this assumption, are based upon the inner and outer connecting body forces F_k^{H} & F_{k+1}^{H} (as shown in Figure 7). The system will then have an increased number of degrees of freedom as a consequence of the action of removing the constraints. This necessitates additional dynamic equations corresponding to the additional degrees of freedom. In fact these additional equations will be those equations eliminated in Section 2.3.5 when establishing Equation (27). The desired generalised constraint force and moment will occur in the modified dynamic equations to be presented. It is also necessary in this procedure to utilise the relative angular velocity components and relative translation speeds between bodies as the generalised speeds. As a consequence the generalised constraining force and moment components will occur singly in each equation and are uncoupled. The final form of the equations to be solved is algebraic.

Under the condition that anchor movements do occur the known generalised speeds to be addressed are:

$$\dot{x}_l : l = 1,2,3 \;\&\; 3r+1, 3r+3 \;\&\; 3N+2, 3N+3, \ldots, 6N \;\&\; r = 1,2,\ldots,N-1.$$

Denoting by F_l^{C} the undetermined generalised constraint forces and eliminating the constraints temporarily will lead to the dynamic equations:

$$a_{lp}\ddot{x}_p = f_l + F_l^{\mathrm{C}} \quad : l = 1,2,3,3r+1, 3r+3, 3N+2, 3N+3, \ldots, 6N; r = 1,2,\ldots,N-1 \;\&\; p = 1,2,\ldots,6N. \tag{48}$$

Next the generalised speeds relating to hinge constraints are set to zero, that is:

$$\dot{x}_l = 0 \ : l = 1,2,3 \ \& \ 3r + 1,3r + 3 \ \& \ 3N + 2,3N + 3, \dots ,6N \ \& \ r = 1,2, \dots , N - 1. \tag{49}$$

Huston then demonstrates, through the application of Equation (2) for the Euler parameter and recognition of the conditions that $s_{12} = 0; s_{13} = 0; s_{ki} = 0 : k = 2,3, \dots , N \ \& \ i = 1,2,3$ indicated after Equation (16) of Section 2.3.4, that:

$$F_l^{\mathrm{C}} = \begin{cases} 0 & : l = 5,8,11, \dots , 3N - 1 \ \& \ 3N + 1 \\ a_{lp}\ddot{x}_p - f_l & : l = 1,2,3 \ \& \ 3r + 1, 3r + 3 \ \& \ 3N + 2, 3N + 3, 3N + 4, \dots ,6N; \\ & \ r = 1,2, \dots , N - 1 \ \& \ p = 5,8,11, \dots ,3N - 1 \ \& \ 3N + 1 \end{cases} \tag{50}$$

For the condition of an anchor temporary fixed or locked the assignment of F_l^{C} is similar with minor changes in the range of values of *l* and *p*.

After determining the unknown generalised speeds and generalised coordinates (together with the associated Euler parameters and translational variables) using Equations (27) to (29) the generalised constraint forces will be obtained on the basis of the Equation (50). The practical constraints assumed regarding anchor chain and restraining cable correspond to smooth hinge joints in the simulation model. Consequently there is no constraining moment (damping moment). Since only the constraint forces exist at the body joints, let F_{km}^{C} and T_{km}^{C} represent the components of principal constraint force vector and moment acting on the centroid of B_k in the inertia reference frame, then analogous to Equations (21) & (23) we have:

$$F_l^{\mathrm{C}} = v_{klm}F_{km}^{\mathrm{C}} + \omega_{klm}T_{km}^{\mathrm{C}} \ : l = 1,2, \dots , 6N; \ k = 1,2, \dots , N \ \& \ m = 1,2,3. \tag{51}$$

Since within equation (51) the number of unknowns equals the number of equations the required quantities F_{km}^{C} and T_{km}^{C} can be determined. However, it should be appreciated that the F_{km}^{C} components do not define the constraint forces at the joints, but correspond to the components of the resultant force acting at the centroid of the selected element. Therefore, the components of the constraint forces F_{km}^{H} at the joint between B_k and its inner connected rigid body are:

$$F_{km}^{\mathrm{H}} = -\sum_{i=k}^{N} F_{im}^{\mathrm{C}} \ : m = 1,2,3 \ \& \ k = 1,2, \dots , N. \tag{52}$$

3.2.3 Forces on ship

Since the presence of water waves is not included, the forces acting on the ship are primarily the weight G_N, the tension $-F_N^{\mathrm{H}}$ acting through the auxiliary rod, the buoyancy force F_N^{B}, the hydrostatic restoring forces F_i^{R} and the current force F^{W}. Assigning m_N and ∇ to represent the ship mass and displaced volume the gravity and the buoyancy forces are:

$$G_N = m_N g \tag{53}$$

and

$$F_N^{\mathrm{B}} = \rho \nabla g. \tag{54}$$

The origin of the inertia reference frame is located at the centroid of the ship water plane. In general the ship hydrostatic restoring forces and moments are expressed as:

$$F_i^{\mathrm{R}} = -C_{ij}x_j^{\mathrm{s}} \ : i, j = 1,2, \dots ,6. \tag{55}$$

Here, $x_j^{\mathrm{s}} : j = 3,4 \ \& \ 5$ correspond to the heave, roll and pitch motions of the ship. Since there is no Archimedean restoration in the horizontal plane, the hydrostatic restoring coefficient matrix $\{C_{ij}\}$ is defined as:

$$\{C_{ij}\} = \begin{bmatrix} 0 & 0 & 0 & 0 & 0 & 0 \\ 0 & 0 & 0 & 0 & 0 & 0 \\ 0 & 0 & \rho g A_{\mathrm{W}} & -\rho g A_{\mathrm{W}} \bar{y}_{\mathrm{f}} & \rho g A_{\mathrm{W}} \bar{x}_{\mathrm{f}} & 0 \\ 0 & 0 & -\rho g A_{\mathrm{W}} \bar{y}_{\mathrm{f}} & \rho \nabla g G_x^{\mathrm{M}} & 0 & 0 \\ 0 & 0 & \rho g A_{\mathrm{W}} \bar{x}_{\mathrm{f}} & 0 & \rho \nabla g G_y^{\mathrm{M}} & 0 \\ 0 & 0 & 0 & 0 & 0 & 0 \end{bmatrix}. \quad (56)$$

The zero elements indicate there is no restoring stiffness associated with surge, sway and yaw and no hydrostatic coupling with heave, roll and pitch. The principal parameters of the matrix are the ship water plane area A_{W}, the ship water plane centroid coordinates $\bar{x}_{\mathrm{f}}$ & $\bar{y}_{\mathrm{f}}$ and the ship transverse and longitudinal metacentric heights G_x^{M} & G_y^{M}.

Assuming z_{B} and z_{G} are the vertical distances of the centre of buoyancy and gravity from the ship keel, then G_y^{M} can be expressed as:

$$G_y^{\mathrm{M}} = z_{\mathrm{B}} + L_N^3 w_N / (12\nabla) - z_{\mathrm{G}}. \quad (57)$$

Because the origin of the inertia reference frame coincides with the ship water plane centroid then $\bar{x}_{\mathrm{f}} = \bar{y}_{\mathrm{f}} = 0$. Since the roll motion is not considered in the two dimensional model the hydrostatic restoring force in its simplest form is:

$$\boldsymbol{F}^{\mathrm{R}} = \begin{bmatrix} 0 & 0 & \rho g A_{\mathrm{W}} x_3^{\mathrm{s}} & 0 & \rho g G_y^{\mathrm{M}} x_5^{\mathrm{s}} & 0 \end{bmatrix}^{\mathrm{T}}. \quad (58)$$

The Reynolds number, Re, of the ship is:

$$\mathrm{Re} = v_{wx} L_N / \vartheta, \quad (59)$$

subject to v_{wx} denoting the longitudinal component of the relative velocity between the ship and the current and ϑ denoting the kinematic viscosity coefficient of the seawater. The ITTC frictional resistance coefficient is

$$C_{\mathrm{f}} = 0.075 / (\log \mathrm{Re} - 2)^2. \quad (60)$$

The hull surface roughness is addressed through the frictional resistance compensation coefficient defined as:

$$C_{\mathrm{sf}} = \left[105 \left(\frac{k_{\mathrm{s}}}{L_N} \right)^{\frac{1}{3}} - 0.64 \right] \times 10^{-3}, \quad (61)$$

with $k_{\mathrm{s}} = 150 \times 10^{-6}\mathrm{m}$ denoting the characteristic height of roughness (Molland et al. 2011). The ship resultant longitudinal drag force, dependent upon ship wetted surface area S_{w}, is expressible as:

$$F_x^{\mathrm{W}} = (C_{\mathrm{f}} + C_{\mathrm{sf}}) \rho S_{\mathrm{w}} v_{wx} |v_{wx}|. \quad (62)$$

3.3 Energy relationship in system

The total energy or work done on the system includes: the kinematic energy E^{K}, the gravitational potential energy E^{G}, the elastic potential energy E^{E} resulting from the hydrostatic restoring forces, the work W^{F} done in overcoming the friction between the gravity anchor and the seabed, the work W^{S} done when mooring elements are wholly or partially immersed in the seabed treated as an elastic foundation and the work W^{C} done by the current force acting on the gravity anchor, the anchor chain, the restraining cable and the ship.

Let E_0 denote the energy of the system at the initial time, then based on the law of conservation of energy, E_0 can be expressed as:

$$E_0 = E^{\mathrm{K}} + E^{\mathrm{G}} + E^{\mathrm{E}} - W^{\mathrm{F}} - W^{\mathrm{S}} - W^{\mathrm{W}}. \tag{63}$$

The kinematic energy in system can be expressed as:

$$E^{\mathrm{K}} = \frac{1}{2}\sum_{k=1}^{N}\left\{m_k\left[\left(\boldsymbol{v}_1^{(0k)}\right)^2 + \left(\boldsymbol{v}_3^{(0k)}\right)^2\right] + I_{k22}^{\mathrm{C}}\left(\omega_2^{(0k)}\right)^2\right\}. \tag{64}$$

Taking the seabed as the zero potential energy surface, the gravitational potential energy in the system satisfies:

$$E^{\mathrm{G}} = \sum_{k=1}^{N}\left(m_k g - F_k^{\mathrm{B}}\right)h_k, \tag{65}$$

with h_k representing the distance from the centroid of body B_k to the seabed. The elastic potential energy E^{E} resulting from the hydrostatic restoration associated with heave and pitch is:

$$E^{\mathrm{E}} = \rho g\left[A_{\mathrm{W}}(x_3^{\mathrm{s}})^2 + G_y^{\mathrm{M}}(x_5^{\mathrm{s}})^2\right]/2. \tag{66}$$

Assume that N_t is the total number of the time steps investigated at time t and d_{1r}^x is the distance travelled by the gravity anchor along the x_0-axis during the r^{th} time step, then the work W^{F} done in overcoming friction between the anchor and the seabed is:

$$W^{\mathrm{F}} = \sum_{r=1}^{N_t} F_1^{\mathrm{F}} d_{1r}^x. \tag{67}$$

Let N_{s} be the number of elements in contact with the seabed. During the r^{th} time step d_{kr}^z is the vertical movement of the centroid of the seabed located element B_i along the z_0-axis. The work W^{S} done in embedding the partially submerged element in the elastically modelled seabed is:

$$W^{\mathrm{S}} = \sum_{r=1}^{N_{\mathrm{t}}}\sum_{k=1}^{N_{\mathrm{s}}} F_k^S d_{kr}^z. \tag{68}$$

The work W^{W} done by the current acting on the ship and all the elements associated with the restraining system (apart from the auxiliary rod) is:

$$W^{\mathrm{W}} = \sum_{r=1}^{N_t}\left(F_x^{\mathrm{W}} d_{Nr}^x + F_1^{\mathrm{D}} d_{1r}^x\right) + \sum_{k=2}^{N-2}\sum_{r=1}^{N_t}\left\{\left(T_k^{\mathrm{A}} + T_k^{\mathrm{D}}\right)\theta_{kr} + \left[F_k^{\mathrm{A}} + F_k^{\mathrm{D}}, 0, F_k^{\mathrm{V}}\right]\boldsymbol{S}^{(0k)}\left[d_{kr}^x, 0, d_{kr}^z\right]^T\right\}. \tag{69}$$

Within W^{W} the parameter d_{Nr}^x is the ship movement during the r^{th} time step and θ_{kr} is the angular displacement of the k^{th} body during the r^{th} time step.

3.4 Computational process

Having completed the presentation of the formulation of the theoretical analysis, the numerical calculation flow chart of the two-dimensional restraining system is depicted as Figure 8.

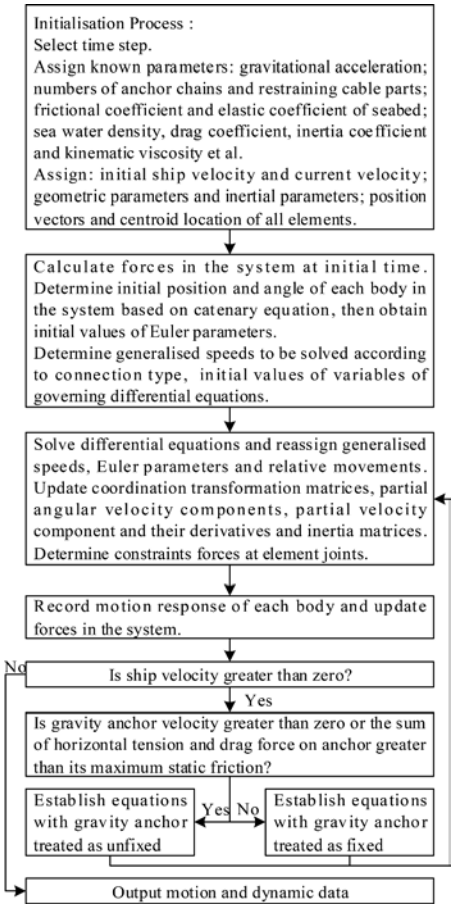

Figure 8. Numerical calculation flow chart for two dimensional restraining system

4. Numerical simulations of retardation system

In order to establish the correctness of the two-dimensional restraining system model developed predictions based on the algorithmic approach of Figure 8, are compared with corresponding results generated through application of the MSC ADAMS (Automatic Dynamic Analysis of Mechanical Systems) software. ADAMS is based on a Lagrange equation formulation.

4.1 Model parameters

In the 2D computations, the integration time step is set at $\Delta t = 0.002\text{s}$. The standard physical parameters required are gravitational acceleration, $g = 9.81\text{m} \cdot \text{s}^{-2}$; seawater density, $\rho = 1025\text{kg} \cdot \text{m}^{-3}$; kinematic viscosity of seawater, $\vartheta = 1.05 \times 10^{-6}\text{m}^2 \cdot \text{s}^{-1}$; steel density, $\rho_s = 7850\text{kg} \cdot \text{m}^{-3}$. The single concrete anchor mass in Figure 2 is twice the mass of each anchor in Figure 1 and set to equal 40t, 50t and 60t with an anchor length corresponding to 2.0m, 2.5m and 3.0m. The anchor width and height are 4.0m and 2.1m in each case.

The mass per unit length of the studless anchor chain in the full-scale retardation system is m_{CU}. The equivalent radius of the single cylindrical representation of an anchor chain element in the 2D model is $R_{\mathrm{CE}} = \sqrt{2m_{\mathrm{CU}}/(\pi\rho_{\mathrm{s}})}$. The parameters of studless anchor chains for different diameters are shown in Table 1. Each length of anchor chain link is 1m long and its whole length is 15m.

Table 1 Studless anchor chain parameters on different diameters (Chakrabarti 2005)

Anchor Chain Diameter (m)	Unit Mass m_{CU} ($\mathrm{kg \cdot m^{-1}}$)	Equivalent Radius R_{CE} (m)	R4 Proof Load (kN)	R4 Break Load (kN)
0.060	71.756	0.0763	2709	3866
0.068	91.741	0.0863	3423	4885
0.076	116.000	0.0970	4205	6001

In the retardation system of Figure 1, the upper restraining cable consists of 19 twisted strands of steel within a high-density polyethylene (HDPE) protective outer sheath. The steel strands have a diameter of 7mm and the unit mass of the upper restraining cable is $m_{\mathrm{RU}} = 6.9\mathrm{kg \cdot m^{-1}}$. The middle and bottom restraining cables, as well as the connection cables are made of high-modulus polyethylene (HMPE). Hence they are light and are used to ensure the ship is duly snared by the retardation system. In the 2D equivalent system of Figure 2, only the upper restraining cable is considered. Hence the equivalent radius for the restraining cable in the 2D model is approximately $R_{\mathrm{RE}} = \sqrt{2m_{\mathrm{RU}}/(\pi\rho_{\mathrm{s}})} = 0.0237\mathrm{m}$ and its break load is 2520 kN. Here the factor of '2' in the R_{RE} deduction is to account for cable attached to two anchor chains in Figure 1. Each element length of three parts of restraining cable illustrated in Figure 2 is of length 2m, 10m and 2m respectively. The different restraining cable lengths addressed in the analyses are 152m, 172m and 192m. The auxiliary rod can be seen as an extended part of restraining cable, thus it has the same material, radius and unit mass, but a shorter length of 1m.

In reality, the ship draught and the centre of gravity (CoG) vary with different loading conditions. Furthermore, the longitudinal stability of a ship, as measured by G_y^{M}, is generally large; see Equation (57). For the convenience of this preliminarily theoretical study the ship is treated as a cuboid with dimensions of $50\mathrm{m}$ by $10\mathrm{m}$ by 5m. The ship CoG is assumed to coincide with the centroid of the water plane area. As illustrated in Figure 2, d_x and d_z respectively denote the horizontal and vertical distances from the joint between the ship and auxiliary rod to the ship water plane centre. The seawater velocity is consistent with the positive x_0-axis. Based on the parameter variations described the distinct cases to be analysed are summarized in Table 2.

Table 2 Expression of Cases

Case	Frictional coefficient	Gravity anchor mass (t)	Equivalent anchor chain radius (m)	Cable length (m)	Cable horizontal component (m)	Cable vertical component (m)	Initial ship velocity ($\mathrm{m \cdot s^{-1}}$)	Ship Mass (t)	Seawater velocity ($\mathrm{m \cdot s^{-1}}$)
1	0.3	40	0.0763	152	148	6	3	500	0
2	0.5	40	0.0763	152	148	6	3	500	0
3	0.7	40	0.0763	152	148	6	3	500	0
4	0.3	50	0.0763	152	148	6	3	500	0
5	0.3	60	0.0763	152	148	6	3	500	0
6	0.3	40	0.0863	152	148	6	3	500	0
7	0.3	40	0.0970	152	148	6	3	500	0
8	0.3	40	0.0763	172	168	6	3	500	0
9	0.3	40	0.0763	192	188	6	3	500	0
10	0.3	40	0.0763	152	149	6	3	500	0

11	0.3	40	0.0763	152	150	6	3	500	0
12	0.3	40	0.0763	152	148	8	3	500	0
13	0.3	40	0.0763	152	148	10	3	500	0
14	0.3	40	0.0763	152	148	6	4	500	0
15	0.3	40	0.0763	152	148	6	5	500	0
16	0.3	40	0.0763	152	148	6	3	750	0
17	0.3	40	0.0763	152	148	6	3	1000	0
18	0.3	40	0.0763	152	148	6	3	500	1
19	0.3	40	0.0763	152	148	6	3	500	2

4.2 Validation of Kane based predictions

The first task is to establish the consistency and veracity of the Kane based analysis of the proposed simplified retardation system. In section 3.3 the initial total energy of the ship, by virtue of its steady advance through the water was equated, through appealing to the principle of energy conservation.

Figure 9 provides the time variation of total energy for those scenarios associated with:

- Increases in water depth (cases 12 &13)
- Higher ship speeds (cases 14 & 15) and
- Larger ship displaced mass (cases 16 & 17)

together with the initial case 1 scenario. The energy variations corresponding to the other cases are not depicted here because they are the same as or only have a little difference with that in case 1. The very minor total energy variation are illustrated in Figure 9. Actually, the relative variation of total energy with respect to initial total energy of the system for those scenarios are all less than 0.5%. This is essentially a result of the accumulated rounding and truncation errors associated with the constituent energy terms defined by Equations (64) to (69) during their numerical evaluation. The authors consider this variation as both reasonable and acceptable, which means the energy is conserved and the consistency of the energy calculation method is validated.

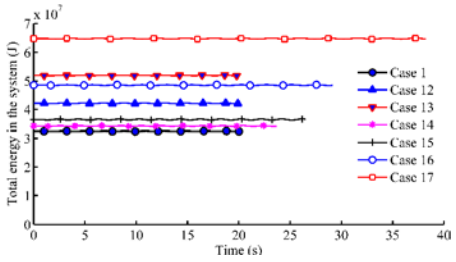

Figure 9. Variation of total energy in the system for selected cases

Having established conservation of total energy the next task is to establish confidence in the Kane based analysis procedure through a comparative study of predicted system element characteristics of horizontal velocities, angular & vertical velocities and joint constraint force (tension) based on the MATLAB implemented Kane method and the Lagrangian formulation based ADAMS code for case 1 alone.

Having observed that the ADAMS related records of angular velocity and vertical velocity were particularly noisy a MATLAB Type I Chebyshev low pass filter was applied to both sets of predictions for case 1; the object of the validation process. The filter had less impact on the MATLAB generated response time series based on the Kane

analysis.

Throughout the different analyses to be addressed the anchor is treated as element 1, elements 2 to 16 represent the anchor chain and elements 17 to 19 model the first stage of the retardation cable as displayed in Figure 2. The second cable stage is made up of elements 20 to 31 in all cases except cases 8 & 9 when element numbers become 20 to 33 and 20 to 35 respectively. Hence the third cable stage has elements 32 to 44, 34 to 46 and 36 to 48 in general, in case 8 and in case 9 respectively. Throughout the last two elements are the ship-cable connection via the auxiliary rod and the ship itself designated 45 & 46, or 47 & 48 or 49 & 50 depending upon the case sensitive division of the second cable stage.

All elements within both simulation methods are tracked for validation purposes. Examination of all suggests it is sufficient to restrict presentation of predictions to those situations which require explanation of retardation system behavioural characteristics, or, demonstrate the influence of a parameter change.

The first observation to note is that both simulation techniques predict 20 seconds are required to stop the ship. Validation of the Kane approach will now be demonstrated by considering motion and force characteristics at the anchor(1), the central elements of the chain (9), cable 1st stage (18), cable 2nd stage (26), cable 3rd stage (38) and the ship (46). The comparisons presented are all for the initial retardation system set up designated case 1.

Figure 10 (a) to (f) provide the horizontal velocities at the stated key representative system elements.

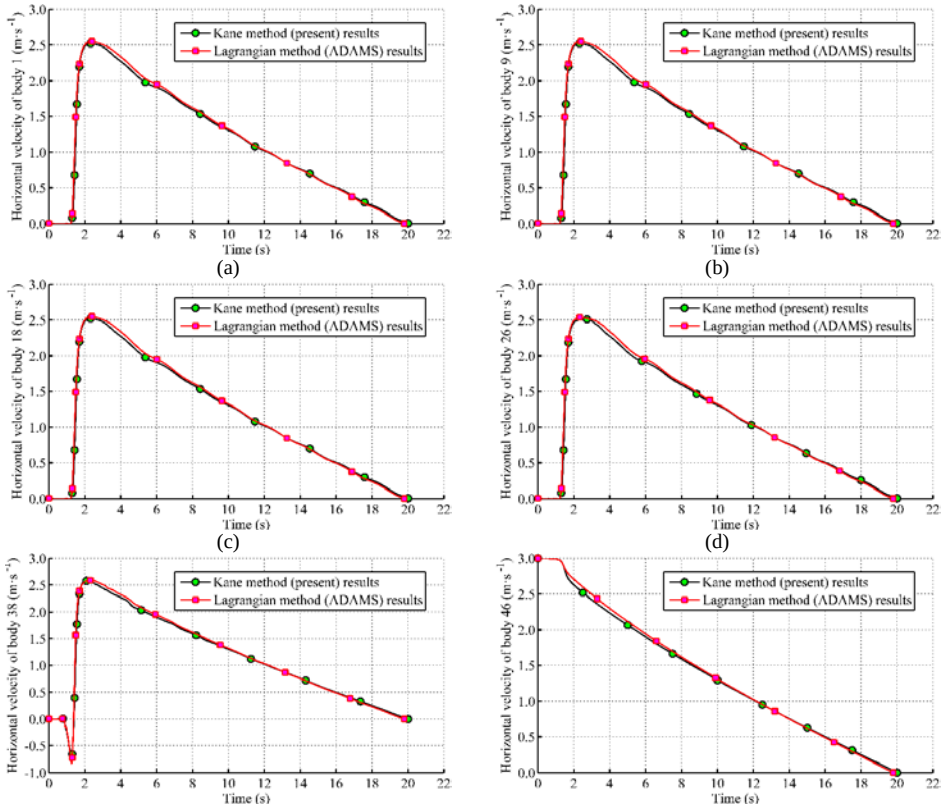

(e) (f)

Figure 10. ADAMS & Kane based predictions of horizontal velocity for representative elements

Prediction of horizontal velocity by both methods is essentially identical and illustrates that horizontal movement of the other elements lag behind the ship movement. The behaviour in the first 2 seconds of the central element of the cable third section indicates some overshoot behaviour. Possible reasons for this are discussed after presentation of Figure 13, when essentially all case 1 representative results have been presented.

Anchor angular velocity is identically zero as expected and therefore not presented. For all chain elements and the elements of the cable first stage all angular velocities are readily bounded by $\pm 1.15^{o}\text{per s}$ $(\pm 0.02 \text{ rad per s})$ for first second of simulation and thereafter reduces to insignificant variations about zero for rest of simulation in each application. The observed differences in chain and first cable predictions are not meaningful in engineering terms.

Figure 11 (a) to (d) provide ADAMS & Kane estimates of angular velocity for a reduced number of representative elements given anchor, anchor chain and first cable section are essentially void of any angular velocity.

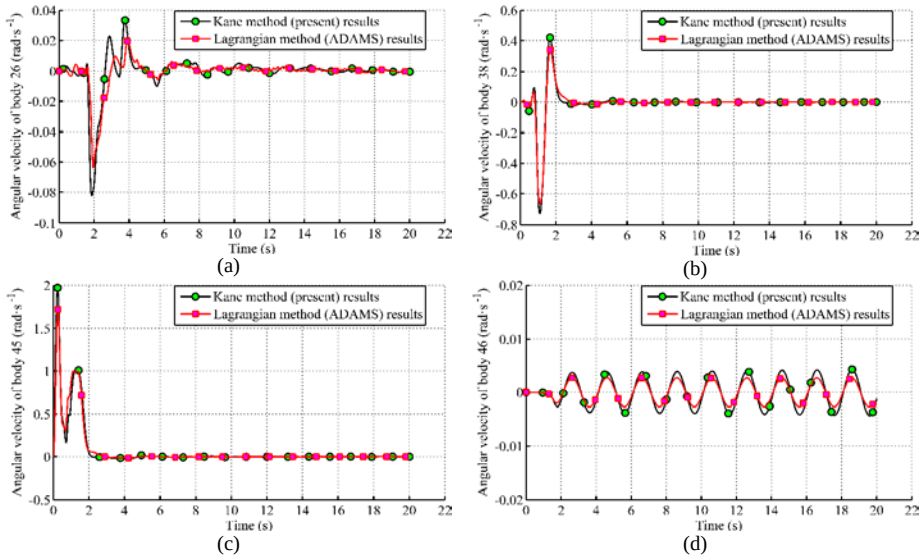

Figure 11. ADAMS & Kane based predictions of angular velocity at representative elements

The ship angular velocities are essentially negligible with peak differences between the two methods being of the order of one thousandth of a radian per second (0.057^{o} per s). Figure 11 shows very close agreement between the two sets of predictions. The angular velocities indicate the rotation of the different elements and hence modification of the associated cable catenary and chain movements relative to the seabed. Advancement of the ship leads to energy transfer to the other elements. It is observable in Figure 11 that whereas the rotation of the ship is clearly negligible there is some high initial rotation in the auxiliary rod which influences the central elements of cable stages 2 and 3. The degree of rotation reduces significantly in those elements further from the ship.

Anchor vertical velocity is identically zero. For the whole of the chain and the cable first stage agreement of zero vertical velocity is predicted within both simulations. Figure 12 (a) to (d) therefore only compare vertical velocity for the central cable elements of stages 2 & 3 together with that of the auxiliary rod and the ship.

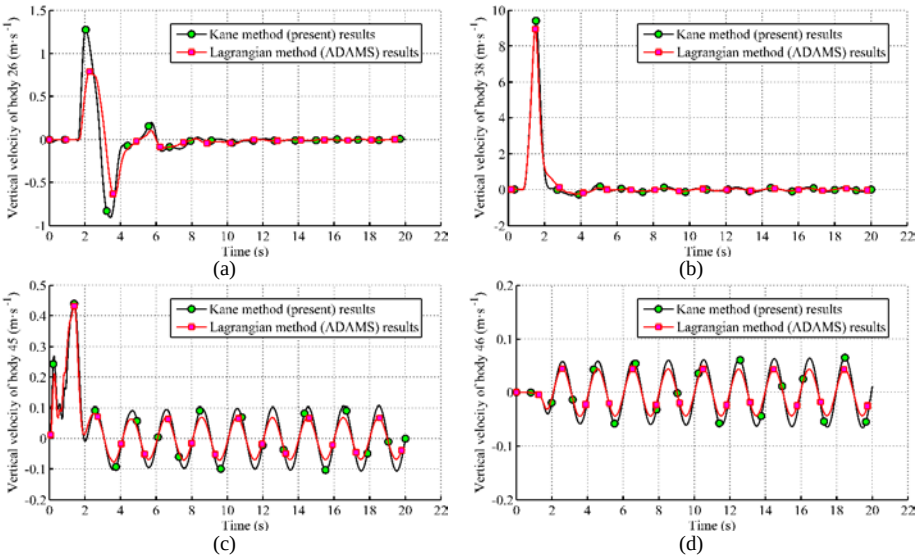

Figure 12. ADAMS & Kane based predictions of vertical velocity at representative elements

Differences between the two procedures exist within the first 4 seconds of the simulation for the central elements of the second stage portion of cable. As we move up the cable the differences in the peak values is about $0.47\mathrm{m}\cdot\mathrm{s}^{-1}$ and then to a negligible difference at the central element of the third cable section. From a practical engineering perspective the steady state auxiliary rod and ship peak differences are very small (between 0.01 and $0.035\mathrm{m}\cdot\mathrm{s}^{-1}$). The energy transfer from ship to other elements is via the auxiliary rod, thereafter the predicted vertical velocity reduces as the elements are located further from the ship.

In Figure 13 the attributed element on the ordinate axis denotes the backward member of the pair of elements involved. Thus element 2 in Figure 13(a) relates to anchor and the first chain link. Figure 13 (b) relates to last chain element and the first cable element. Figures 13(c) & (d) provide joint tension at the cable stage 2 & 3 central elements, that is, at the junction of elements 25 & 26 and 38 & 39 respectively. Finally the behaviour of auxiliary rod & ship is displayed in Figure 13(e).

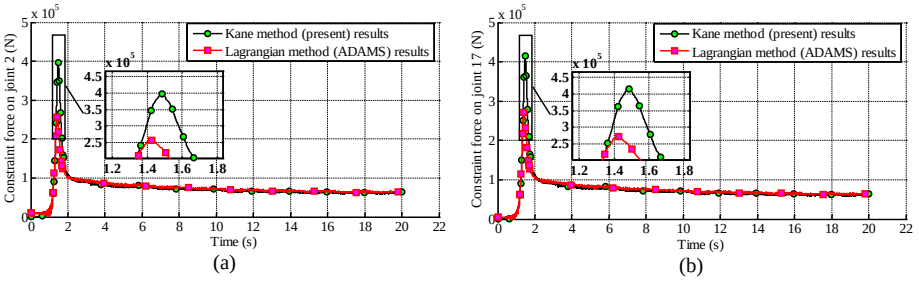

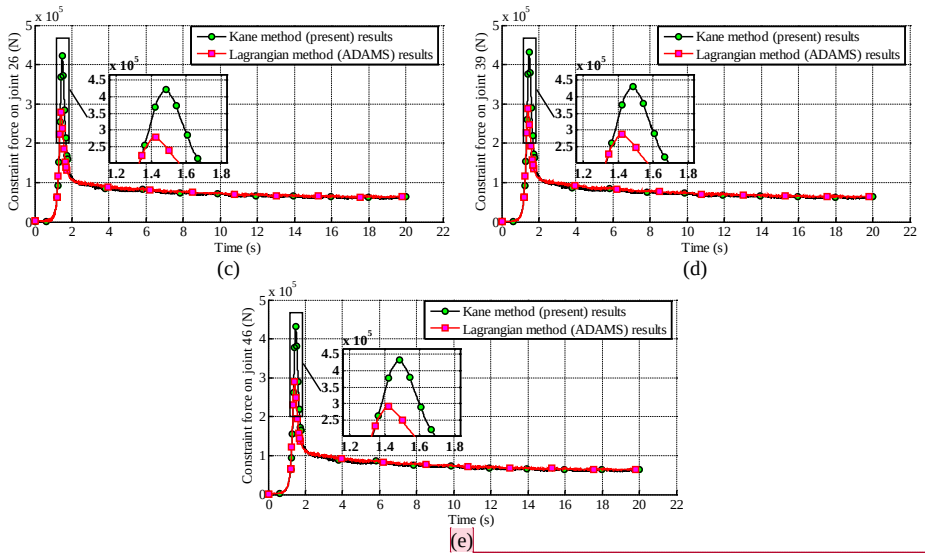

Figure 13. ADAMS & Kane based predictions of constraint forces at representative joints

Commented [l1]: Whether need a subtitle for each figure?

Other than 'hairbreadth' increases in peak tension values the behaviour for all other chain link joints are essentially identical to Figure 13(a). Parts (b) to (e) indicate the same trends independently of element location whether considering tension variation with time over the 20 second retardation period or comparing the exploded peak tensions in the associated superimposed thumb sketches.

Clearly the peak tensions based on the Kane formulation and that predicted by the ADAMS software are distinct. Identification of a reason for these differences is difficult given element definition is identical in setting up each procedure and all quantities requiring assignment or specification of the calculation procedure for associated physical parameters are treated identically and thus consistently. The only difference is thus the mathematical formulation of the governing equations.

The principal source of these peak responses of different physical quantities is thought to be the sudden forced anchor movement due to energy from the ship being transferred to the anchor through the other elements of the retardation system. In the initial state, only the ship moves, and with its motion other cable and chain elements begin to move sequentially and reach a reasonably similar velocity. When the motion transfers to the anchor, it has to move suddenly and reach a similar velocity to the other elements. Within the reported simulations forces are applied at 100% of the calculated value. When examining the behaviour of moored offshore structures it is usually the practice to ramp up the applied forces from a small percentage to fully calculated values over a significant earlier portion of the simulation. This approach is to prevent numerical shocks leading to excessive unrealistic motions (Hearn et al. 1988). Here there are no real environmental influences other than the reactions to the presence of water. This in part explains the relatively short duration of the numerical shock created.

The large peaks in the validation figures presented should be considered as numerical shock within the simulation. Physical observation of the selected ship subjected to use of the proposed retardation system is required to establish what proportion of these predicted peaks are physical. Clearly, at some early point in the activation of the retardation system, a snatch load is taking place whose influence diminishes with time.

From a structural integrity viewpoint the difference in peak joint constraint force predictions and the level of the associated higher peak force predictions in these figures are small compared with the associated chain proof load and cable breaking loads defined in Section 4.1.

In all the figures presented the time step has been maintained at 0.002 seconds throughout for both methods. It is assumed that the coefficients in the MATLAB implementation of the Runge Kutta process used comply with the Butcher Tableau conditions (Butcher 1963 and 1996). To ensure integration time step is acceptable different time steps were examined for the MATLAB implemented Kane analysis. Figure 14 provides recalculated Kane predictions corresponding to the results presented in Figure 13 (e) based on application of alternative integration time steps.

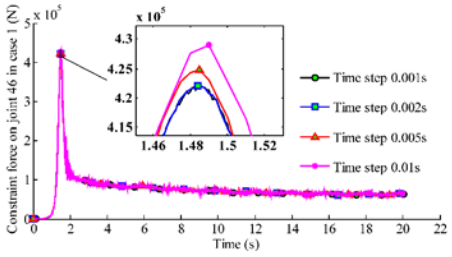

Figure 14. Kane based predictions of constraint force at ship based on different integration time steps

Clearly the original selected time step is not an issue in this case.

4.3 General study of retardation system responses

Having established the consistency of the Kane and ADAMS predictions in general for each physical quantity over many representative elements the Kane predictions alone have been used to appreciate the significance or otherwise of retardation system and ship related parameter changes set out in Table 2. Comparisons are always considered relative to the initial formulation of case 1. However, where predicted differences in selected quantities are too small for meaningful identification of differences predictions will not be explicitly presented. It was evident in Figures 10 through 13 that in many cases the behaviour at different elements was not particularly significant. Hence there will be situations in which significantly less graphical information needs to be presented.

This phenomenon applies to the parameter variations associated with anchor chain radius variation (comparison of cases 1, 6 & 7), variation in cable overall length (cases 1, 8 & 9 compared), minor changes in horizontal cable length and vertical cable length leading to comparison of case 1 with cases 10 & 11 and 12 & 13 respectively. In each case (except in the cases 8 & 9, where the constraint force peaks are affected) variation of different velocity components, translations and tension variations within each set are negligible both numerically and in engineering pertinence terms. These same cases are shown not to significantly affect the stopping time of the ship as illustrated in Table 3.

Table 3 Stopping time for cases defined in Table 2

Case	Stopping time (s)	Parameter change
1	20.010	None
2	13.228	Seabed friction increased
3	10.054	

4	16.774	Anchor mass increased
5	14.498	
6	19.992	Anchor chain radius increased
7	19.976	
8	19.972	Overall cable length increased
9	19.936	
10	19.702	Minor changes in horizontal projected length of cable
11	19.386	
12	19.908	Minor changes in cable vertical length
13	19.798	
14	23.654	Initial ship speed increased
15	26.516	
16	29.134	Ship displaced mass increased
17	38.242	
18	22.122	Introduction of current flow influence
19	24.126	

4.3.1 Influence of variable seabed frictional coefficient upon responses

In cases 2 & 3 of Table 2 all variables except frictional coefficient are invariant; that is μ initially set as 0.3 is now increased to 0.5 and then 0.7 respectively. However μ is still assumed constant over the sea floor. As a consequence of indicated increases in μ the retardation period is significantly reduced from 20.01 seconds to 13.23 seconds and 10.05 seconds.

Figures 15 to 18 inclusively provide minimal representative system responses to indicate the more important changes within the retardation system elements.

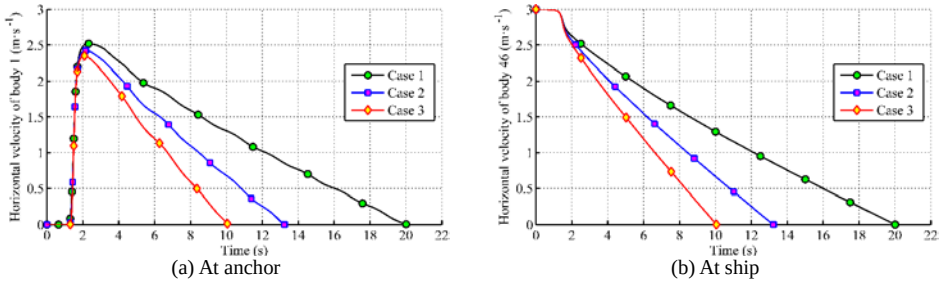

(a) At anchor (b) At ship

Figure 15. Kane based predictions of horizontal velocity for cases 1, 2 & 3

Figure 15 illustrates the expected phase shift between anchor velocity and ship velocity. It takes approximately 1.5 seconds before anchor movement occurs. Hence during this initial time interval the ship velocity is constant approximately. The increased seabed frictional coefficients clearly reduce the time required to stop the ship.

The corresponding horizontal translations of anchor and ship are presented in Figure 16. Translations of cable central elements are essentially no different to variation of the anchor translations illustrated. Figure 16 indicates that the translations of element in the system drop nonlinearly with the frictional coefficient increment.

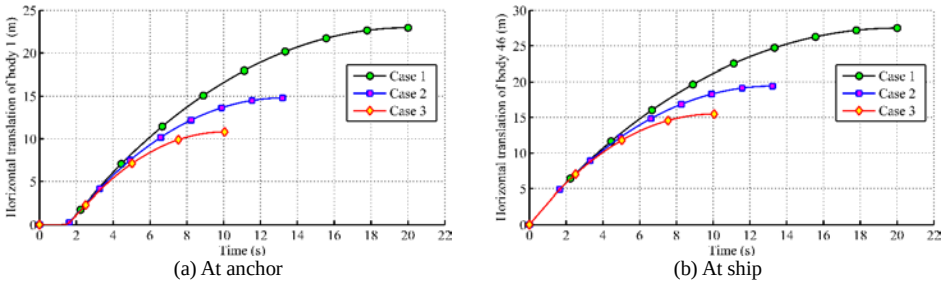

(a) At anchor (b) At ship

Figure 16. Kane based predictions of horizontal translation for cases 1, 2 & 3

Anchor angular velocity is zero throughout. For all chain elements and cable first stage elements peak angular velocities are bounded by $\pm 1.42^{o}\text{per s}$ $(\pm 0.025\,\text{rad per s})$ and observed differences in response are not particularly meaningful in terms of engineering significance. That is, variation is no different to that presented in Figure 11 for case 1. Therefore we next consider in Figure 17 the vertical velocity variation of cable third sector central element and that of the ship.

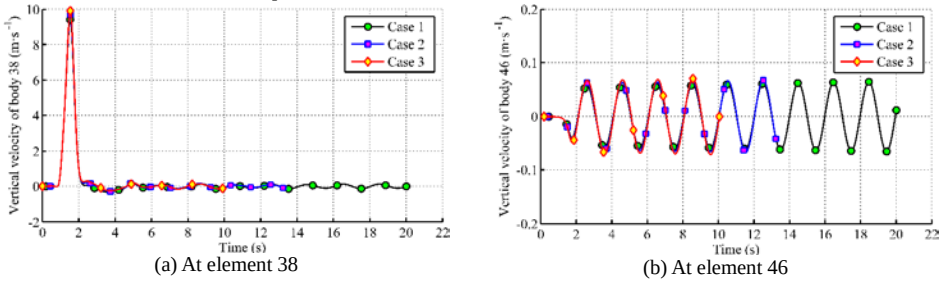

(a) At element 38 (b) At element 46

Figure 17. Kane based predictions of vertical velocity for cases 1, 2 & 3

The ship vertical velocity is always bounded and oscillatory. The third cable central element continues to experience the high initial single peak observed in Figure 12 by both the ADAMS and Kane predictions. Thereafter each simulation equally settles to small bounded values. The physically unexpected high initial peaks are considered to be associated with initial numerical shock in the simulations as discussed after Figure 13.

Variations of the joint constraint forces, illustrated in Figure 18, are very similar in behaviour and amplitude irrespective of joint location within the retardation system. Hence only the constraint force between anchor and anchor chain is displayed. It shows that the constraint force peak value is affected by the frictional coefficient. The peak approximately goes up linearly with the increase of frictional coefficient.

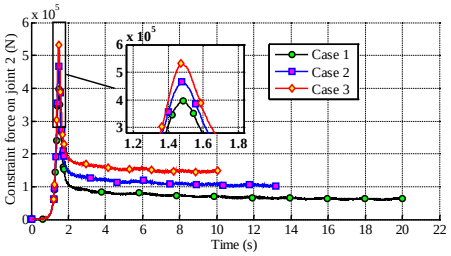

Figure 18. Kane based predictions of constraint forces for cases 1, 2 & 3 at anchor / first anchor chain link joint

4.3.2 Influence of anchor mass increase upon responses

For cases 4 & 5 anchor mass is increased from 40 tonnes to 50 and 60 tonnes respectively. All other variables remain unchanged. Comparison of plots of angular velocity and vertical velocity variations with time for the three anchor masses considered (cases 1, 4 & 5) indicate negligible differences at any instant in time. Hence only horizontal velocity, horizontal translation and constraining forces are presented in Figures 20 to 22 respectively for limited element positions.

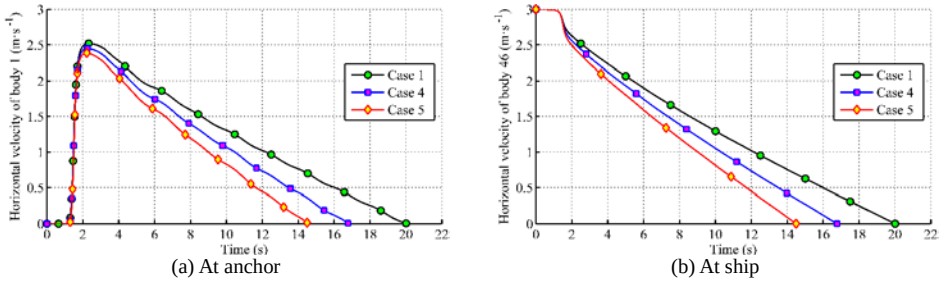

(a) At anchor (b) At ship

Figure 19. Kane based predictions of horizontal velocity for cases 1, 4 & 5

Anchor mass increases are effective in shortening the duration of the retardation process. The peak horizontal velocities here are compatible with the corresponding increased frictional coefficient peak values of Figure 15. The duration in this case is not reduced to the same extent as frictional coefficient increases (see Table 3 too).

Observations regarding the horizontal translations now presented in Figure 20 are extremely similar in magnitude to those of Figure 16 apart from the variation corresponding to a slower completion of the retardation process over slightly larger distances. Predictions for anchor and ship alone are illustrated as behaviour of other retardation system elements is the same as that of the anchor.

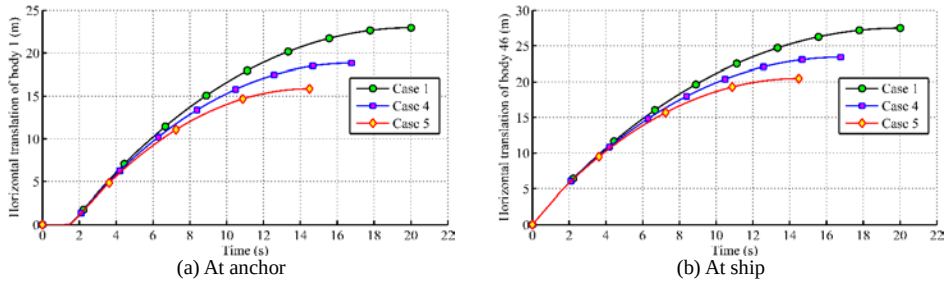

(a) At anchor (b) At ship

Figure 20. Kane based predictions of horizontal translation for cases 1, 4 & 5

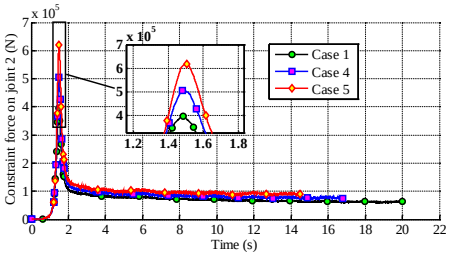

Figure 21. Kane based predictions of constraint forces for cases 1, 4 & 5 at anchor / first anchor chain link joint

Figure 21 indicates that peak joint tension behaviour is approximately 15% larger than that displayed in Figure 18 and the anchor weight also makes the peak increase. However there is minor variation in joint tension variation in Figure 21 from 3 seconds onward, whereas the steady state levels in Figure 18 were distinct for each frictional coefficient value.

4.3.3 Negligible influence of anchor radius and cable dimensions upon responses

Whilst comparison of cases 1, 6 & 7 were essentially invariant to the variation of chain radius it is worth noting that the peak constraint forces in this case are comparable with Figure 13. As already indicated, variation of cable geometric parameters in the case groupings of 1, 8 & 9 and 1, 10 & 11 produced no predictions significantly different to case 1. For cases 1, 12 & 13, the water depth changes only make an obvious effect on the maximum constraint forces, which will be shown in Section 4.3.7 later.

4.3.4 Influence of ship initial speed upon responses

For cases 14 & 15 initial ship velocity is changed from $3\mathrm{m}\cdot\mathrm{s}^{-1}$ to $4\mathrm{m}\cdot\mathrm{s}^{-1}$ and then $5\mathrm{m}\cdot\mathrm{s}^{-1}$. All other variables remain invariant. Clearly total energy in the system increases in this case and hence the retardation process will be longer and the distances travelled greater.

Again angular velocity variations are so indifferent that the related figures will not be presented. Figures 22 to 25 will therefore present horizontal velocity, horizontal translation, vertical velocity and joint tension variations at selected elements.

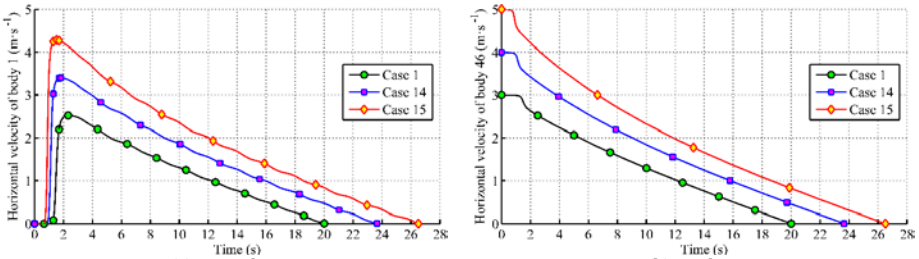

(a) At anchor (b) At ship

Figure 22. Kane based predictions of horizontal velocity for cases 1, 14 & 15

Figure 22 clearly indicates that peak horizontal velocity and stopping time have increased as expected. The anchor horizontal speed increase is of the order of 85% for the highest ship speed.

Figure 23 indicates that the ship distance travelled in the retardation process has raised linearly with the increase of ship speed.

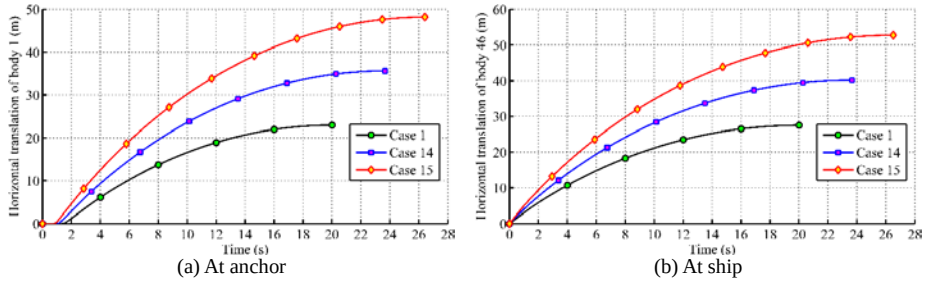

(a) At anchor (b) At ship

Figure 23. Kane based predictions of horizontal translation for cases 1, 14 & 15

Figure 24 reinforces the vertical velocity characteristics shown in Figure 17. The oscillation is essentially of similar frequency but of larger amplitude for the higher ship speeds. From Figure 24(a), it shows the numerical shock peaks related to vertical velocity increase with the ship speed. For other cable section central elements the magnitude of the peaks is significantly smaller and beyond 5 seconds the vertical velocity is small and similar to that associated with the ship vertical velocity in Figure 24(b).

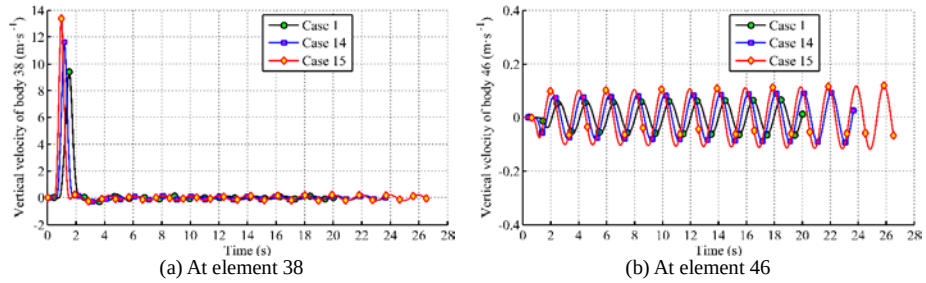

(a) At element 38 (b) At element 46

Figure 24. Kane based predictions of vertical velocity for cases 1, 14 & 15

Variation of constraint force is only evident in the peak tensions that persist for the first few seconds in Figure 25. Compared with earlier peak tensions they are nearly 2.2 times larger in this case. Occurrence of peaks in this case is at different earlier times as the initial ship speed of advance is increased. In corresponding Figures 18 & 21 the peak joint forces occurred at essentially the same instant in time.

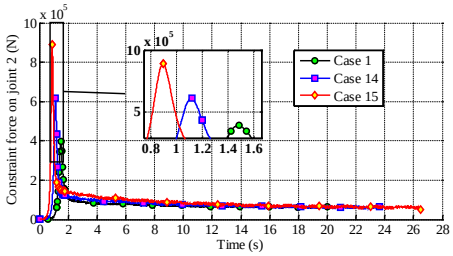

Figure 25. Kane based predictions of constraint forces for cases 1, 14 & 15 at anchor / first anchor chain link joint

4.3.5 Influence of ship displacement upon responses

For cases 16 & 17 ship mass is increased by 50% and then 100% to given ship displaced masses of 750 & 1000 tonnes. All other variables remain invariant. Figures 26 and 27 indicate large increases in duration of retardation process (see Table 3) and increased distances travelled by anchor and ship. The ship with the largest displacement is now approximately taking twice as long to stop.

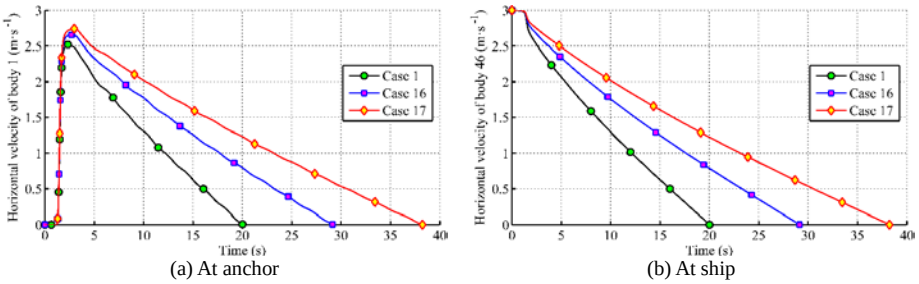

(a) At anchor (b) At ship

Figure 26. Kane based predictions of horizontal velocity for cases 1, 16 & 17

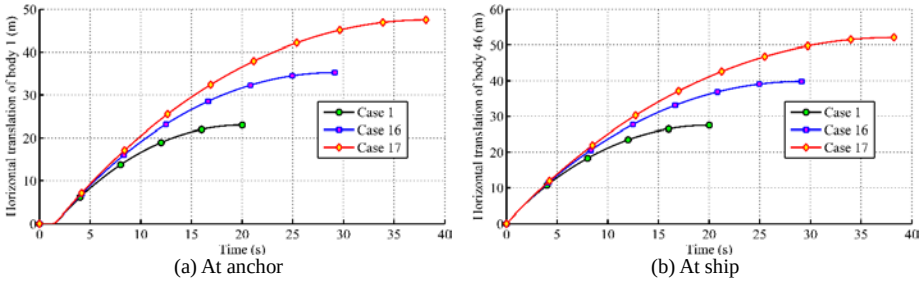

(a) At anchor (b) At ship

Figure 27. Kane based predictions of horizontal translation for cases 1, 16 & 17

Vertical velocity in this case reflects the large 3rd cable section central element peaks of Figures12, 17 & 24. The amplitudes in Figure 28 (a) indicate that ship displacement has little influence on these numerical shock related peaks. Ship vertical velocities in Figure 28 (b) are smaller than those of Figure 24 but otherwise show the same displaced oscillatory behaviour.

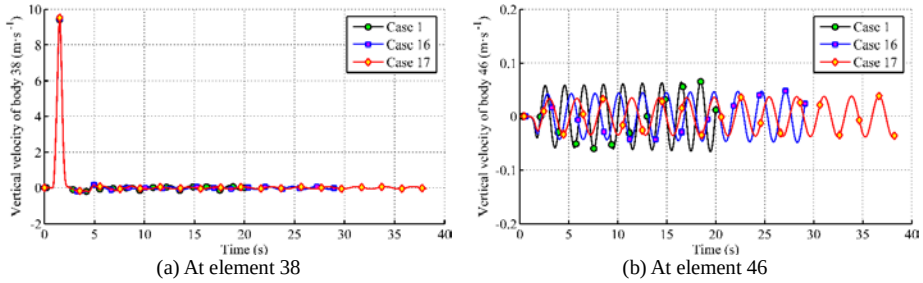

(a) At element 38 (b) At element 46

Figure 28. Kane based predictions of vertical velocity for cases 1, 16 & 17

Joint constraint forces in Figure 29 are not particularly influenced by the increased displaced mass of the ship. Peak tensions increased in Figure 25 are now back to nominal levels of earlier parametric studies.

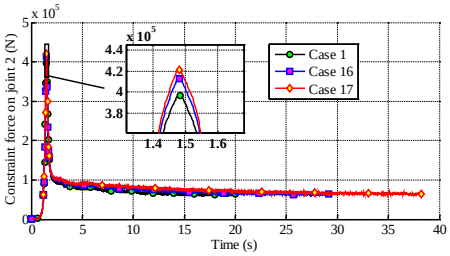

Figure 29. Kane based predictions of constraint forces for cases 1, 16 & 17 at anchor / first anchor chain link joint

4.3.6 Influence of steady current upon responses

The next comparison looks at the influence of the introduction of a steady current flowing in the same direction as the original ship heading. The variation of both angular velocity and vertical velocity for cases 18 & 19 relative to case 1 are negligible and therefore their time variation plots are not presented. Figures 30 to 32 therefore provide horizontal velocity, horizontal translation and joint constraint force variations respectively. Since the current effectively provides a driving force the retardation process takes longer.

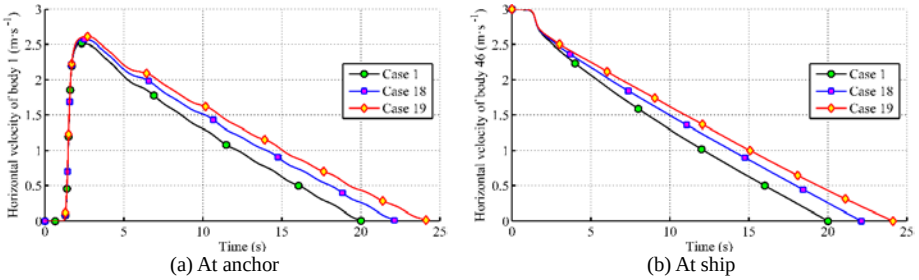

(a) At anchor (b) At ship

Figure 30. Kane based predictions of horizontal velocity for cases 1, 18 & 19

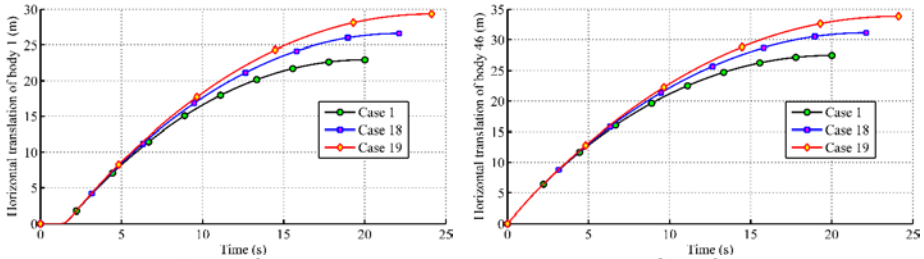

(a) At anchor (b) At ship

Figure 31. Kane based predictions of horizontal translation for cases 1, 18 & 19

Figures 30 & 31 show that uniform currents lead to more distance covered over a longer time period.

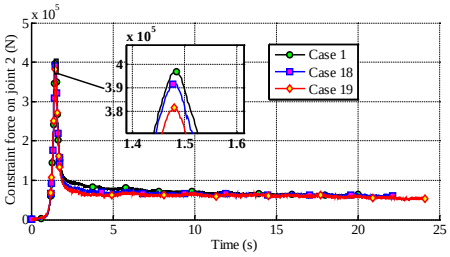

Figure 32. Kane Based Predictions of constraint forces for cases 1, 18 & 19 at anchor / first anchor chain link joint

The uniform currents have a little influence on the joint constraint forces.

4.3.7 Maximum constraint force responses

The joint constraint peak forces clearly presented in Figures 13 and 14 will occur when undertaking an investigation of parameter sensitivity of the retardation to its system changes or ship parameter modifications. Having observed throughout the early peaks in the various responses within the retardation system, Figure 33 presents the maximum joint constraint forces for the different parameter scenarios addressing friction, anchor mass, water depth, initial ship velocity, ship displacement mass and current influences.

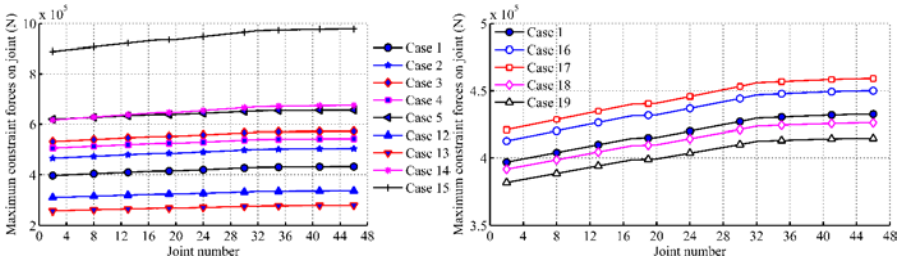

(a) For cases with evident effects (b) For cases with a little effect

Figure 33. Maximum constraint forces of all elements for some selected cases

Figure 33(a) indicates that the constraint peaks are influenced significantly by frictional coefficient, anchor mass, water depth and initial ship velocity. In particular, the maximum constraint forces are much greater and also vary more in case 15, which demonstrates the maximum forces are sensitive to the influence of ship initial velocity. From Figure 33(b), it can be seen that the ship displacement mass and current have a little effect on the peaks, whilst the other parameters (anchor chain radius, cable length and its horizontal projected length) have no influence on the maximum values and thus are not presented. Besides, for each case, the maximum tensions become increasingly big at the "higher numbered" joints, this is because the element joint (with a larger number) needs to supply greater forces to make the lower elements move.

5. Conclusions

The simplified 2D analysis of a proposed overhead retardation system to stop an advancing ship without propulsion power has been analysed using reduced Kane equations. Validation of the proposed Kane based analysis has been established using the Lagrangian based ADAMS software. The only differences between the two simulation processes is the governing equations; all constituent equations and parameter specifications are identically specified

within each simulation.

Observed higher peaks within the few seconds of each simulation are considered the result of numerical shock arising from all forces being applied as calculated rather than being steadily ramped as time advances. The magnitudes of these initial peaks are well below the proof stress of the chain selected and the yield stress of the cable assigned. The initial peaks arise because the ship provides the energy transferred through the retardation system. Since the initial condition assumes anchor, anchor chain and catenary cable are in static equilibrium the rapid transfer of ship energy to anchor movement is the primary cause of these early peaks in element behaviour. Catenary theory can be applied to approximately analyse the responses of the retardation system, but the dynamic influences will not be addressed. The Kane method permits a detailed study of the impact of anchor movements upon the performances of the retardation system. This approach is also useful for future investigations of the impact of the variation of seabed frictional characteristics.

Extensive parameter sensitivities have been reported based on the Kane approach only. These studies demonstrate that variations in anchor chain, overall cable length or its horizontal projected length have no real impact on the retardation behaviour. Section 4.1 indicates that chain length is fixed at 15m and the restraining cable is very long ($\geq$ 152m). Clearly if cable length were significantly reduced the dynamics would change and hence the retardation system behaviour would be radically modified. The parameter changes related to sea bed friction, anchor mass, water depth, initial ship speed and increased displaced ship mass (associated with increased cargo) do impact upon system dynamic responses. The angular velocity and vertical displacement of each system element is less affected in general than horizontal motion and movement and joint restraint forces.

The wide range of parameter changes investigated illustrates the feasibility of the proposed retardation system on the ship of assumed real characteristics. A full 3D analysis is required to demonstrate the overhead retardation system proposed in Figure 1. Testing of ship corresponding to that used in the simulation with due comparison of measured and predicted behaviour is the next step in this ongoing research.

Acknowledgments

The authors would like to thank the National Natural Science Foundation of China (NSF) under Grant No. 51679250 and 51379213, the National Key Technology R&D Program (Grant No. 2014BAB16B05) and High-tech Ship Research Projects Sponsored by Chinese Ministry of Industry and Information Technology for financially supporting this research.

The authors also gratefully acknowledge the China Scholarship Council (CSC) support for related research hosted at the University of Southampton.

References

1. Butcher JC. 1963. Coefficients for the study of Runge–Kutta integration processes. Journal of the Australian Mathematical Society, 3 (2), 185–201. doi: 10.1017/s1446788700027932

2. Butcher JC. 1996. A History of Runge-Kutta methods. Applied Numerical Mathematics, 20(3), 247-260. doi:10.1016/0168-9274(95)00108-5

2. Chakrabarti S. 2005. Handbook of Offshore Engineering . Elsevier.

3. Chang ZY, Tang YG, Li HJ, Yang JM, Wang L. 2012. Analysis for the deployment of single-point mooring buoy system based on multi-body dynamics method. China Ocean Engineering 26(3): 495-506. doi:10.1007/s13344-012-0037-x

4. Chen XJ, Huang GY, Wu GH, Shi J. 2009. Energy balance relationship in collision between ship and moored collision-prevention system. [in Chinese.] Journal of PLA University of Science and Technology (Natural Science Edition) 10(1): 71-76. doi:10.7666/j.issn.1009-3443.20090113

5. Chen XJ, Huang GY, Wu GH, Tang XF. 2013. Numerical simulation for the motion of the flexible floating collision-prevention system. Journal of Offshore Mechanics and Arctic Engineering 135(1): 011303. 1-9. doi:10.1115/1.4006763

6. Fan W, Yuan WC. 2014. Numerical simulation and analytical modeling of pile-supported structures subjected to ship collisions including soil–structure interaction. Ocean Engineering 91: 11-27. doi:10.1016/j.oceaneng.2014.08.011

7. He B, Tang W, Cao JT. 2014. Virtual prototyping-based multibody systems dynamics analysis of offshore crane. The International Journal of Advanced Manufacturing Technology 75(1-4): 161-180. doi:10.1007/s00170-014-6137-4

8. Hearn GE, Lau SM, Tong KC. 1988. Wave drift damping influences upon the time domain simulations of moored structures. OTC Paper 5632, 2-5 May, Houston, Texas, ISBN 978-1-61399-081-0 doi:10.4043/5632-MS

9. Huston RL, Kamman JW. 1981. A representation of fluid forces in finite segment cable models. Computers & Structures 14(3-4): 281-287. doi:10.1016/0045-7949(81)90013-4

10. Huston RL. 1990. Multibody Dynamics. Massachusetts: Butterworth-Heinemann.

11. Jiang H, Chorzepa MG. 2015. Evaluation of a new FRP fender system for bridge pier protection against vessel collision. Journal of Bridge Engineering 20(2): 05014010. 1-12. doi:10.1061/(asce)be.1943-5592.0000658

12. Jiang H, Chorzepa M G. 2016. Case Study: Evaluation of a Floating Steel Fender System for Bridge Pier Protection against Vessel Collision. Journal of Bridge Engineering 21(11): 05016008. 1-14. doi:10.1061/(ASCE)BE.1943-5592.0000947

13. Jiang ZB, Shao LZ, Shao F. 2015. Numerical simulation of the spreading dynamic responses of the multibody system with a floating base. Journal of Marine Science and Application 14(3): 290-301. doi:10.1007/s11804-015-1302-1

14. Kane TR and Levinson DA. 1985. Dynamics: Theory and applications. New York: McGraw-Hill book company. ISBN: 0-07-037846-0

15. Ku N, Ha S. 2014. Dynamic response analysis of heavy load lifting operation in shipyard using multi-cranes. Ocean Engineering 83: 63-75. doi:10.1016/j.oceaneng.2014.03.026

16. Ma BH, Zhao MH, Zhang L, Lei Y. Analysis on underside friction effect of beam on elastic foundation based on energy principle. [in Chinese.] Journal of the China Railway Society, 2012, 34(4): 94-100. doi:10.3969/j.issn.1001-8360.2012.04.016

17. McNatt JC, Venugopal V, Forehand D. 2015. A novel method for deriving the diffraction transfer matrix and its application to multi-body interactions in water waves. Ocean Engineering 94: 173-185. doi:10.1016/j.oceaneng.2014.11.029

18. Molland AF, Turnock SR, Hudson DA. 2011. Ship Resistance and Propulsion. New York: Cambridge University Press.

19. Mou JM, van der Tak C, Ligteringen H. 2010. Study on collision avoidance in busy waterways by using AIS data. Ocean Engineering 37(5): 483-490. doi:10.1016/j.oceaneng.2010.01.012

20. Qiu A, Lin W, Ma Y, Zhao CB, Tang YH. 2015. Novel material and structural design for large-scale marine protective devices. Materials & Design 68: 29-41. doi:10.1016/j.matdes.2014.12.002

21. Saleh JM. 2002. Fluid Flow Handbook. New York: McGraw-Hill Professional Publishing.

22. Shen Q, Li Y, Chen XJ. 2003. Dynamic analysis of multibodies system with a floating base for rolling of ro-ro ship caused by wave and slip of heavy load. Journal of Marine Science and Application 2(2): 17-24. doi:10.1007/BF02918659

23. Tran TT, Kim DH. 2015. The coupled dynamic response computation for a semi-submersible platform of floating offshore wind turbine. Journal of Wind Engineering and Industrial Aerodynamics 147: 104-119. doi:10.1016/j.jweia.2015.09.016

24. Wang LL, Yang LM, Huang DJ, Zhang ZW, Chen GY. 2008. An impact dynamics analysis on a new crashworthy device against ship–bridge collision. International Journal of Impact Engineering 35(8): 895-904. doi:10.1016/j.ijimpeng.2007.12.005

25. Wang LL, Yang LM, Tang CG, Zhang ZW, Chen GY, Lu ZL. 2012. On the impact force and energy transformation in ship-bridge collisions. International Journal of Protective Structures 3(1): 105-120. doi:10.1260/2041-4196.3.1.105

26. Wang T. 2004. Ocean Engineering (in Chinese), Shandong, China: Shandong Education Press.

27. Wu GH, Yu QL, Chen XJ. 2009. An energy consumed collision-prevention system of long distance anchor moving for non-navigational bridge (in Chinese), Highway (1): 213-218. http://www.cnki.com.cn/Article/CJFDTotal-GLGL200901047.htm

28. Xu X, Yang JM, Li X, Xu LY. 2015. Time-domain simulation for coupled motions of three barges moored side-by-side in floatover operation. China Ocean Engineering 29(2): 155-168. doi:10.1007/s13344-015-0012-4

29. Yan B, Dai GL. 2011. Investigation and countermeasures of ship-bridge collision accidents in China in recent years. In: Advanced Materials Research Vol. 168. Switzerland: Trans Tech Publications; 167-174. doi:10.4028/www.scientific.net/AMR.168-170.167

30. Yang K, Wang XY, Ge T, Wu C. 2014. Dynamic model of underwater snake-like robot using Kane's method. Journal of Shanghai Jiao Tong University (Science) 19(2): 146-154. doi:10.1007/s12204-014-1483-9

31. Zhou FH, Yu TX, Yang LM. 2012. Elastic behavior of ring-on-foundation. International Journal of Mechanical Sciences 54(1): 38-47. doi:10.1016/j.ijmecsci.2011.09.005

32. Zhu B, Chen RP, Chen YM, Zhang ZH. 2012. Impact model tests and simplified analysis for flexible pile-supported protective structures withstanding vessel collisions. Journal of Waterway, Port, Coastal, and Ocean Engineering 138(2): 86-96. doi:10.1061/(asce)ww.1943-5460.0000110